DELFT UNIVERSITY OF TECHNOLOGY

MASTER THESIS

Dilating Pupil for Prosthetic Eyes Based on Electrowetting

Jinyi Liu

TU Delft Delft University of Technology

VUmc

Dilating Pupil for Prosthetic Eyes Based on Electrowetting

by

Jinyi Liu

in partial fulfilment of the requirements for the degree of

Master of Science

in Electrical Engineering

at Electrical Instrumentation Laboratory, EWI, Delft University of Technology

Supervisor:	Dr. ir. A. Bossche	
	Jeroen Bastemeijer	
Thesis committee:	Prof. Dr. P. J. French	EWI
	Prof. Dr. ir. K. M. B. Jansen	IO
	Dr. H. W. van Zeijl	EWI


TU Delft
Delft
University of
Technology

Electronic
Instrumentation
Laboratory

EKL
Else Kooi Laboratory

ABSTRACT

The prosthetic eye is created to help people who have lost an eye. The eye itself can only improve the appearance but without any optic function. In order to optimize the appearance, a prosthetic eye with a pupil that can dilate and contract according to the light level, just like the natural eye, is desired. The primary goal of this work is to develop and characterize a dilating pupil based on electrowetting. A droplet of an aqueous solution acts as a pupil.

Electrowetting-on-dielectric (EWOD) has become one of the most popular tools in variety of applications, from microfluidics to electrowetting displays. This thesis presents the design of a low-voltage electrowetting one-pixel display which can act as a pupil. Decreasing the maximum actuation voltage is the main objective and challenge of this project. Different methods to achieve this goal are presented in the thesis, including using dielectric materials with better dielectric properties and using electrowetting liquids with lower surface tension. Ways to minimize the effect of gravity are also investigated. Droplet-based simulations are introduced by two methods. The simulation results are used to sustain the design process and for comparison with the measurement results on the real devices. According to the theoretical background and simulations, a test device is designed and fabricated in the cleanroom of EKL, TU Delft. The fabrication details are described in this thesis. Finally, measurements on the fabricated device are performed under different conditions. The results are shown and discussed in the final conclusions. In general it can be said that an electronic dilating pupil based on EWOD seems possible. Some recommendations for the future improvement are made.

ACKNOWLEDGMENTS

This project lasted for more than one year. During this period of time, I have received countless help from many people.

My most thanks goes to Dr.ir. Andre Bossche, who introduced me to this project and helped me continuously. I am grateful to him for his tolerance. I would also like to thank Jeroen Bastemeijer for helping me from begin to end, especially in setting up the experiments. Furthermore I would like to thank Prof. K.M.B.Jansen for his enthusiastic participation and suggestions, Prof.Dr.P.J.French and Dr.H.W.van Zeijl for sharing their knowledge and experience of the fabrication processes.

I want to thank Gregory, Tom, Jian and Yue for their help in the EKL cleanroom. Special thanks to Violeta for helping with the aluminium oxide deposition. My thanks to Jiahan for his companionship and help during the two years. Moreover, I would like to thank my friends in Delft, especially Guanchu and Jessica.

Finally I would like thank to the many good people that I lucky enough to meet during the two years in Delft, for their friendship and support. I will never forget this experience for all my life. I would like to express my thanks to my parents, for the selfless and endless love and concern.

Jinyi Liu

2018.02.10

CONTENTS

ABSTRACT..... v
ACKNOWLEDGMENTS..... vii
CONTENTS..... ix
Chapter 1 Introduction 1
1.1 Background and Motivation..... 2
1.2 Related Research and the Necessity of This Project..... 3
1.2.1 Self-regulating iris based on light-sensitive liquid crystal elastomer 3
1.2.2 Light-reactive ocular prosthesis based on electroactive polymer (EAP)..... 4
1.2.3 What is a dilating pupil based on Electrowetting technology..... 5
1.3 Patients Feedback on Current Prosthesis..... 6
1.4 Research Challenges and Goals..... 7
1.5 Thesis Outline 7
Reference: 8
Chapter 2 EWOD: Background & Theoretical Analysis..... 9
2.1 Wetting: Contact between Three Phases..... 10
2.1.1 Wetting and Wettability 10
2.1.2 The Young's Equation 10
2.2 Electrowetting Theory 11
2.2.1 Brief History and Theory of Electrowetting 11
2.2.2 Contact Angle Saturation (CAS)..... 12
2.2.3 Contact Angle Hysteresis 13
2.3 Low-voltage EWOD..... 13
2.3.1 Hydrophobic Surface..... 14
2.3.2 Insulating Dielectric..... 15
2.3.3 Electrowetting Liquid and Surface Active Additives 17
2.4 AC vs DC..... 18
2.5 Centralization of the Droplet..... 19

2.5.1 Separate electrodes 19
2.5.2 Coplanar Electrodes 20
2.6 Summary 22
Reference: 23
Chapter 3 Modeling of EWOD 25
3.1 Introduction of the Model 26
3.2 Method Ⅰ: Laminar Two-Phase Flow, Level-set Physics 27
3.3 Method II: Coupled CIR, ES and TPF Multiphysics 28
3.4 Summary 29
Reference: 30
Chapter 4 DESIGN AND FABRICATION 31
4.1 Material Decision 32
4.2 Mask Design 32
4.2.1 Electrode Layer Design 33
4.2.2 Dielectric Layer 'via' Opening 34
4.2.3 Hydrophobic Layer Design 34
4.2.4 Mask Overview and Creation 35
4.3 Basic Microfabrication Techniques 37
4.3.1 Photo Lithography 37
4.3.2 Thin Film Deposition Methods 38
4.3.3 Etching Methods 39
4.4 Fabrication Procedure in the cleanroom of EKL 40
4.4.1 Introduction 40
4.4.2 Cleaning 41
4.4.3 Zero layer lithography and TEOS deposition 42
4.4.4 Lithography, Metallization and Lift Off process 42
4.4.5 Dielectric Deposition and Etching 44
4.4.6 FluoroPel 1601V Patterned method 44
Reference: 47
Chapter 5 Experiments and Results 49
5.1 Experiment Ⅰ: Testing the electrowetting properties of the selected materials 50
5.2 Experiment II: Measurements on the devices with coplanar electrodes 51

5.3 Experiment III: Long-term Test of FluoroPel Reliability 53
Chapter 6 Conclusions and Future Works 55
6.1 Conclusions 56
6.2 Future Work Recommendations 57
Appendix 59
Process Flowchart 59
List of Figures 63
List of Tables 65

Chapter 1

Introduction

This project is aimed to design a dilating pupil for prosthetic eyes based on electrowetting. For people who lose one eye, the prosthetic eyes can help them feel sound. In this chapter, the background and motivation are firstly clarified. Then the related studies performed by others are reviewed and compared with this project to show the advantages of our work. Then based on the feedback of some patients, the objectives and challenges are defined. Finally the outline of this thesis is given.

1.1 Background and Motivation

The human eye is the organ which gives us the sense of light, allowing us to see and interpret the shapes, colours, and dimensions of objects in the world. Eyes are important in almost every activity people perform. However, sometimes because of damages or diseases of the eye, such as severe injury, glaucoma, infection inside the eye and eye tumours, it may be impossible to save the eye and the eyeball must be surgically removed. Inherited conditions are also reasons for eye loss, for instance, microphthalmia and anophthalmia [1]. According to the Society for the Prevention of Blindness, between 10000 and 12000 people per year lose an eye in the world [2].

To help people feel sound as well as improve the appearance after losing one eye, the artificial eyes (shown in **Figure 1-1**) have been designed. For a long time, people have been exploring ways to decorate the loss of eye. Many materials like glass, bone, sponge, fat and precious metals have been used to create implants. Today most artificial eyes are made of acrylic plastic polymer called polymethyl methacrylate (PMMA) which offers best safety and perfect match with a real eye, with an average life of about 10 years [3]. After a surgery to remove the eye from the socket, an implant is then placed into the socket to restore lost volume and to give the artificial eye some movement. So natural movement is not a problem to be concerned. Currently, this kind of artificial eyes can only provide cosmetic enhancement but no function of restoring vision. So after removal of the natural eye and placement of a prosthetic eye, a person will not have vision in that eye.

Figure 1-1 The acrylic artificial eyes with different size, pupil and eye ball color

With the advancements in computer, electronics and biomedical engineering technology, it is possible to improve and develop prosthesis that looks more natural and might even provide sight someday. Work is already in progress to achieve this goal. A Canadian company aims to develop an artificial eye that will be connected to the optical nerve and the visual cortex. This

kind of research will take more years and also need a long-term validation before it can make it to a product [4]. This project aims to provide another approach to create a more natural looking artificial eye which can dilate or contract its pupil according to the light levels. As a part of this long-term project, improvements and optimizations are the main work based on the previous work finished by Ronald van der Beek (2016, TU Delft) as his master thesis [5].

The ocular accommodation system of eyes utilizes the iris to regulate the diameter of the pupil, thereby controlling the amount of light entering the human eye. In order to make the prosthetic eyes more natural, developing a dilating pupil like the real eyes have, has been long cherished wish. Size-controllable image can be easily achieved by many advanced technologies, theoretically. In [5], different technologies are listed and analysed, like LCD, E-Ink, electrowetting, shape memory polymers, thermochromic ink and so on. The final choice is Electrowetting, as it has got some advantages over the others. Electrowetting (EW) phenomenon has recently obtained great attention due to its wide potential of applications, although the initial studies were underway decades ago. This is because of the fact that it is an effect which allows to control the surface tension of the fluids by applying electrical energy. EW is studied and applied widely, such as adjustable liquid lenses, microfluidic actuators, and electronic displays. However, up to now its research and applications are still not yet fully utilized by the existing limited technology.

1.2 Related Research and the Necessity of This Project

Life-reactive prosthetic eyes have been proposed by many researchers. In this chapter, several studies on dilating pupil are reviewed. Technologies like electroactive polymer (EAP) and liquid-sensitive liquid crystal elastomer can achieved pupil dilation according to the light luminosity, which has been studied by the researchers of Tampere University of Technology (TUT) and Nottingham Trent University (UK) [6,7].

1.2.1 Self-regulating iris based on light-sensitive liquid crystal elastomer

The iris in the human eye is a circular structure responsible for controlling the diameter and size of the pupil and thus the amount of the light reaching the retina, ensuring a high-quality vision event. Like the cameras, the pupil is the eye's aperture, while the iris is the diaphragm. The Smart Photonic Materials research group from Tampere University of Technology (TUT) has developed an artificial iris that acts like human eye, using a material that itself is photoresponsive and gives a configuration that opens or closes in response to decreasing or increasing light intensity [6]. A light-sensitive liquid crystal elastomer (LCE) iris was reported that can autonomously open and close as a real iris does without any sensors or mechanisms.

From **Figure 1-2** (a), the aperture (pupil) has a diameter of 14 millimetres and 12 separate petals made from LCE material and painted into red colour. **Figure 1-2** (c) shows the two boundary states of the pupil. In the dark circumstance, the pupil should be wide to allow more light into the eye, and the petals curl upward correspondingly. But as soon as they are exposed to strong light, the petal unfold to reduce the diameter of the pupil.

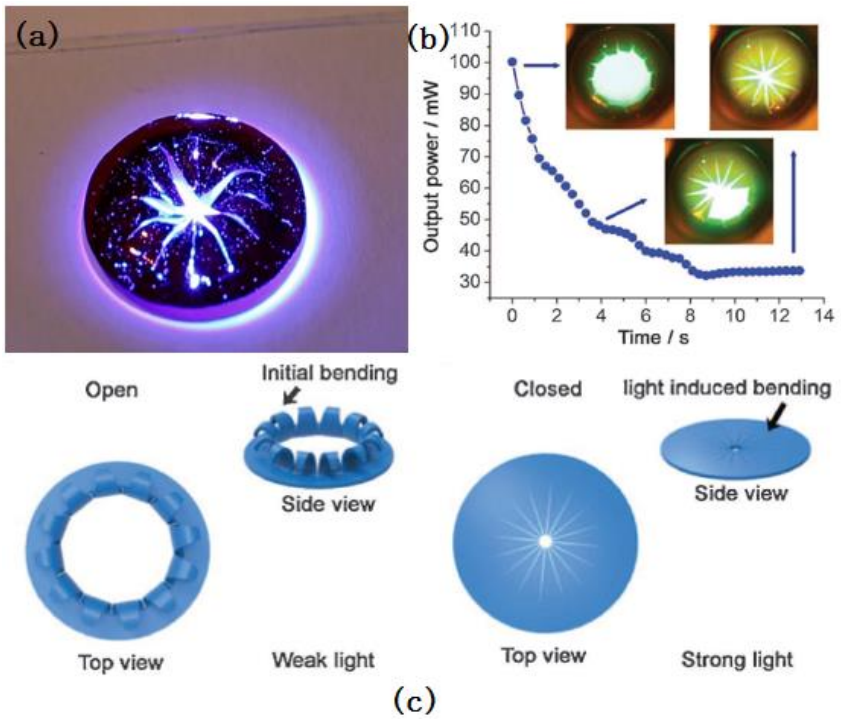

Figure 1-2 (a) The overview of the LCE (b) Different states of the iris responding to different light power (c) Two boundary states of the pupil: under weak light and strong light. [6]

To make it adaptable as an optical implant, sensitivity enhancement will be considered firstly so that its opening and closing can be triggered by smaller changes of the incoming light intensity.

1.2.2 Light-reactive ocular prosthesis based on electroactive polymer (EAP)

Researchers of Nottingham Trent University have created an artificial eye with a cosmetic pupil that can dilate and contract in response to light [8]. This research project is based on utilizing the electroactive polymer (EAP) made from a soft silicone disc with stretchable carbon electrodes on each side [7]. Electroactive polymer technology has notably applied in artificial muscle and soft robotics. Philip and John *et al.* [7] found the visual impression of dilation can be achieved using this technology. When applying a high-voltage across the electrodes, the electrostatic force squashes the disc, making it thinner and wider as shown in **Figure 1-3**. It is an over-sized prototype eye and the voltage needed was 1.5 kV. Increasing

the input voltage provides the image of dilation, while decreasing the voltage provides the image of contraction.

Figure 1-3 An over-sized prototype pupil made from a dielectric elastomer actuator (DEA) [8]

EAP technology makes the combination of the realistic pupil and iris hand-painted possible. However, in this work still much has to be done in size miniaturization as well as reducing the high voltage to a safe range.

1.2.3 What is a dilating pupil based on Electrowetting technology

The gradation project undertaken by Ronald van der Beek (TU Delft) [5] researched a product design of a pupil which can dilate and contract in response to different light levels and integrated in a prosthetic eye. In his report, possible technology that can visually represent dialting and contracting pupils are reviewed and electrowetting technology was finally chosen and studied. The basic model prototype of the project is shown in **Figure 1-4**.

The change of the 'pupil' composed of black aqueous solution is driven by electrowetting effect which will be presented in detail in chapter 2. The work principle is that the photocell behind the pupil responses to different light circumstances, and thus delivers a corresponding signal to a microcontroller which in turn delivers a voltage to the electrodes of the electrowetting device to set the dilation at the right level. According to different voltage levels, the black liquid can change to different sizes just like people's pupil does.

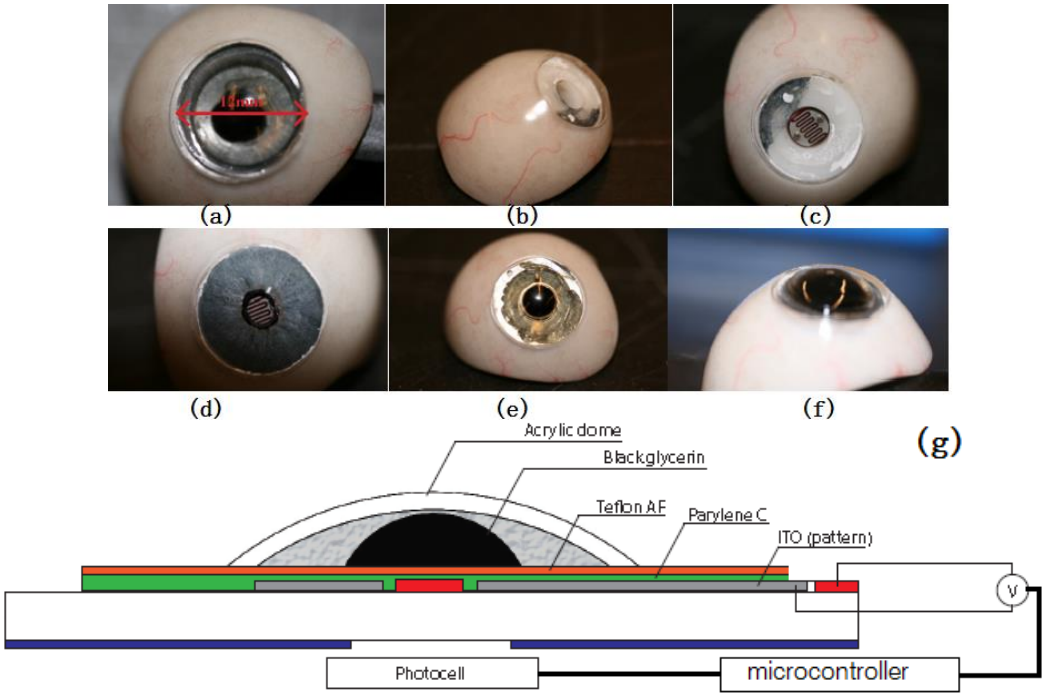

Figure 1-4 The show model prototype schematic and assembly (a) The dimension of the iris; (b) Drilled and milled out prosthetic eye; (c) Light sensor placed inside the eye; (d) A hand-painted iris attached; (e) The electrowetting device placed; (f) Side view of the whole prosthetists; (g) The structure and details of the electrowetting device.

This project is a part of the subsequent work of optimization the electrowetting effect before it can be made a product. Compared to other technology, electrowetting shows some advantages. Unlike EAP technology, electrowetting can be easily scaled down to the natural pupil size and low-voltage requirements. In addition, from the look of the model prototype, electrowetting can provide a more natural look. These advantages make this research valuable and meaningful.

1.3 Patients Feedback on Current Prosthesis

To have a better understanding of how this prosthetic eye work, the patients were visited and gave some feedback with the help of Jelmer Remmers, the ocularist of FrédériqueBak Kunstogen®. The main discussion is as follows.

The 'eye' is specially customized by the ocularist according to the colour and size of patient's eye and can improve the appearance of the affected eye socket, which is better than wearing an eye patch or bandage. However, it would be better if there were techniques that could achieve a dilating pupil inside the eye. Because many people especially children, often stay outdoors with large light variations so that the difference between two pupils is obvious.

It is suggested to wear and remove it every day. And the surface of the prosthesis collects protein and debris. So cleaning it every 2-3 weeks is ideal. It should be professionally polished

every 6 months to provide a comfortable and natural appearance. The artificial eyes also need to be replaced approximately every five years for safety and health reasons.

1.4 Research Challenges and Goals

Since the prosthetic eye is placed in patients' body, safety problem should be primarily considered. The control voltage of the device should be limited in the safe voltage range of human's body, the smaller the better. Meanwhile, a reliable and solid packaging is also necessary.

In order to look as real as possible, many important factors will be taken into consideration, for instance, the response time of the "pupil" to the light intensity change, and the unneglectable gravity influence. Besides, the reliability and sustainability cannot be ignored. The objective of this project is:

- The pupil inside of the prosthetic eye can dilate and contract;
- The driving voltage should be as small as possible;
- The device should be reliable and not do any harm to the user.

1.5 Thesis Outline

The main body of this thesis comprises 6 chapters. **Chapter 2** introduces the electrowetting theory and analyses the possible choices of materials, processes and structures to achieve the goals. **Chapter 3** shows some simulation results in ideal situations and also some simple setup experiments. **Chapter 4** details mask design and the processes flow in fabrication of the substrate. It also describes the fabrication procedures in the cleanroom. **Chapter 5** reports fabrication and measurements results of various parameters which are compared to find the best performance. **Chapter 6** concludes the work done and recommends future aspects for improvement and optimization of the electrowetting device.

Reference:

[1] Knežević M, Paović J, Paović P, et al. Causes of eye removal: analysis of 586 eyes [J]. Vojnosanitetski pregled, 2013, 70(1): 26-31.

[2] Custer P L. Eye Was There: A Patient's Guide to Coping With the Loss of an Eye [J]. 2012.

[3] http://www.madehow.com/Volume-3/Artificial-Eye.html

[4] https://www.the-scientist.com/?articles.view/articleNo/41052/title/The-Bionic-Eye/

[5] Van der Beek R E. Prosthetic eye with dilating pupil[J]. 2016.

[6] http://onlinelibrary.wiley.com/doi/10.1002/adma.201701814/full

[7] Breedon P J, Lowrie J P. Life-like prosthetic eyes: the call for smart materials [J]. Expert Review of Ophthalmology, 2013, 8(4): 315-316.

[8] https://www.electronicsweekly.com/news/research-news/device-rd/smart-pupil-contracts-in-uk-artificial-eye-2013-04/

Chapter 2

EWOD: Background & Theoretical Analysis

The dilating pupil inside the prosthetic eye is designed based on the technology of Electrowetting-on-Dielectric (EWOD). In this chapter, the work principles of electrowetting and EWOD are presented firstly. Based on that, some application issues are discussed, and to prevent failures in the next experiment step, different materials and technology are reviewed to provide a better choice. At last, several ideas to centre the pupil are put forward.

2.1 Wetting: Contact between Three Phases

2.1.1 Wetting and Wettability

After rainfall, water droplets can be seen on leaves of very different shapes. Also, on the windows, there are different shaped droplets. The shapes of the droplets are determined by the degree of the interaction between the droplets and the surface of leaves and windows. This degree is known as **wetting**. Wetting is the ability of a liquid to maintain contact with a solid surface, due to the intermolecular interaction, such as adhesive and cohesive forces [1], between the three phases: vapour (air), liquid (water) and solid (leaves) interface [2-4].

Wettability is a property of a surface that determines how fast a liquid will spread over the surface, indicating the affinity for liquids on a solid surface. It can be defined by different wetting phenomena. The **contact angle** (CA) θ of liquid on the solid surface, measured between the liquid-vapour interface and the solid-liquid interface, is an index of surface wettability, as shown in **Figure 2-1**. A low contact angle ($0 < \theta < 90°$) means high wettability, indicating the wetting of the surface is very favourable and such a surface is called hydrophilic surface, see **Figure 2-1**(a). Likewise, a high contact angle ($90° \leq \theta < 180°$) means low wettability, indicating the wetting of the surface is unfavourable and the surface is called hydrophobic surface, see **Figure 2-1**(b)[1].

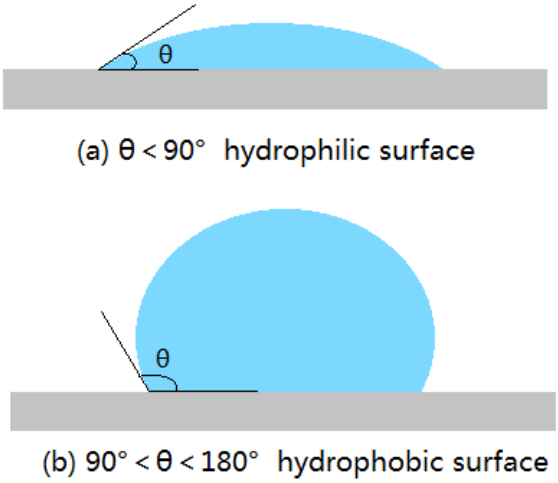

Figure 2-1 Schematic diagrams of contact angle of a liquid droplet on solid surfaces

2.1.2 The Young's Equation

The simplest way to realize the wetting property is to drop a liquid on the surface and measure the contact angle. And in 1805, Young proposed that the contact angle is determined by a balance of interfacial forces at a three-phase contact line [5]. It can be presented by the Young's Equation:

$$\gamma_{sv} = \gamma_{sl} + \gamma_{lv} \cos\theta. \qquad 3.1$$

Where γ_{sv} , γ_{sl} and γ_{lv} are solid-vapour, solid-liquid and liquid-vapour interfacial force per unit length of the contact line which can also be interpreted as surface tension, and θ is the contact angle (see **Figure 2-2**). The interfacial tension γ_{sv}, γ_{sl} and γ_{lv} are dependent on the materials used. The value can be found in the literature. For example, the tension of pure water in air at room temperature is 72.75mN/m.

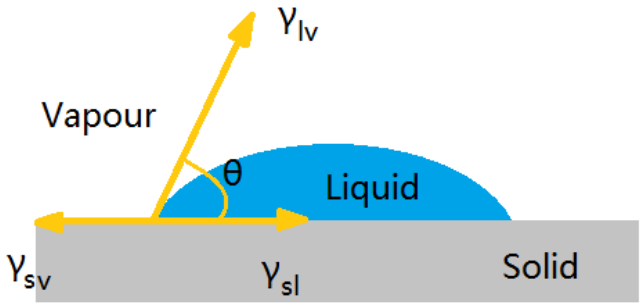

Figure 2-2 Young's Equation for Three-Phase Interfacial Tension (θ is the contact angle, γ_{sv} is the surface tension of solid-vapour surface, γ_{sl} is the surface tension of solid-liquid surface, γ_{lv} is the surface tension of liquid-vapour surface)

Young's equation has been defined for an ideal surface, i.e. perfectly flat, chemically and physically homogenous, in absence of gravity and no contact angle hysteresis [6].

2.2 Electrowetting Theory

2.2.1 Brief History and Theory of Electrowetting

These surface properties of solids cannot be changed easily without chemical treatment. However, from the 1980s, the discovery and development of electrowetting allowed to modify the surface properties by applying electric fields.

Electrowetting is a microfluidic phenomenon, which can be defined as the manipulation of the surface wettability with an electric field. In 1875, Gabriel Lippmann in his PhD dissertation reported that the capillary depression of a mercury- in contact with the electrolyte solutions- could be varied by applying a voltage between the mercury and the electrolyte solutions [7]. This phenomenon is called electro-capillarity and is the basis of the modern electrowetting. In the next several decades, this phenomenon was studied continuously. However, electrolysis occurred and formed a problem when the applied voltage was beyond a hundred millivolts in the early study of electrowetting, which was the main reason obstructing the applications. In 1993, Berge introduced a 12 μm thickness Parylene film as an insulating layer between the substrate and the liquid to eliminate electrolysis problems. In contrast to the former experiments, Berge's experiment required approximately 170 volts. This improved form of electrowetting was referenced as electrowetting-on-dielectric (EWOD) [8].

Berge also proposed the EWOD equation based on Young's and Lippmann's theories called Lippmann-Young equation:

$$\cos\theta(V) = \cos\theta_0 + \frac{\varepsilon}{2\gamma_{lv}d}V^2 \qquad 3.2$$

$\theta(V)$	Contact angle under a certain voltage		
V	The electric voltage	ε	The dielectric constant of the dielectric material
θ_0	Initial contact angle	d	The thickness of the dielectric film

A typical schematic of an EWOD system is presented in **Figure 2-3**. A droplet of an aqueous solution is dropped on a thin dielectric film covering an electrode. Around the droplet is immiscible fluid like oil, or gas, like air. When an electric field is applied across the system, the electric charge is built at the interface between the conductive liquid and the electrode seen as the **Figure 2-3** (d). Then the dielectric layer can be seen as a capacitor and the surface tension is reduced by the capacitive energy. The capability of controlling the contact angle by applying a potential allows electrowetting technology to be used in a wide range of application, such as liquid lens and electronic displays.

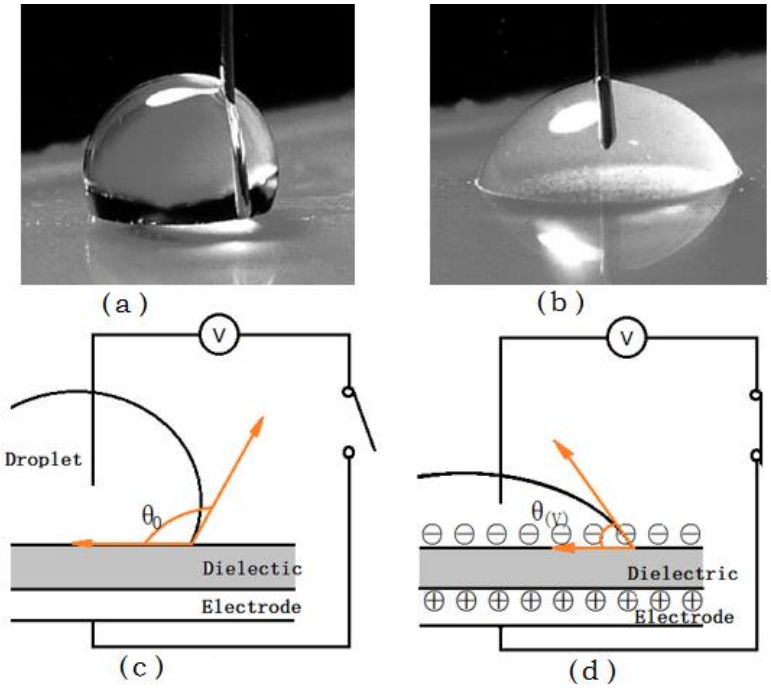

Figure 2-3 Schematic of electrowetting-on-dielectric. (a, c) No external voltage applied: the droplet is a round shape and contact angle is more than 90 degree. (b, d) External voltage applied: charge density changes so that the contact angle decrease or increase.

2.2.2 Contact Angle Saturation (CAS)

According to the electrowetting equation, if all parameters remain the same, the contact angle is directly changed by the applied voltage. So it is easy to draw a conclusion that the contact angle can reach zero, which means full wetting, with a sufficient large voltage. However, the fact is that even very large external voltages fails to achieve full wetting. A number of experiments show that, for small voltages, the contact angle decreases with increasing voltages according to the Young-Lippmann equation. However, as the voltage is above a certain value,

the electrowetting contact angle starts to deviate from the equation and saturates. This phenomenon is known as **Contact Angle Saturation** (CAS).

There are no exact explanations about the mechanism of this phenomenon. In the last few decades, the contact angle saturation have been given a numbers of interpretations:

A. Dielectric charging: The charges trapped in the insulator, when the voltage becomes larger, reduce the concentration of the charges at the solid-liquid surface [9, 10].

B. Ions injection from an aqueous droplet into its surrounding oil or air: The Maxwell stress is arising, when the charges carried by ions are accumulated at the interface of the water-oil (or air) phase. The increasing injected charges from droplet to oil decreases the Maxwell stress at the water-oil interface so that the CAS occurs [9, 11].

C. The electric resistance of the droplet: The liquid is not perfectly conductive with zero resistance. The resistance depends on the shape of the droplet that the resistance is increasing with the droplet spreading [9, 12]. (This interpretation mainly matters in AC operation.)

Besides these three aspects, other physical reasons are involved when the CAS is occurring, but based on the previous studies, the dominant reason is time-dependent, with different mechanisms dominating the saturation behaviour over different time scales.

2.2.3 Contact Angle Hysteresis

Electrowetting is analog and reversible. When starting to apply voltage from zero, the advancing contact angle with increasing voltage is different from the retreating contact angle when reducing the voltage at the same point. This difference is called contact angle hysteresis [6, 13, 14]. This is because of different reasons, for example, the surface roughness and the characteristic of the surface chemistry.

2.3 Low-voltage EWOD

The idea of using electrowetting has been investigated by many researchers in recent years. In most studies, a thick dielectric film (more than 10 μm) was used. So the voltages required to generate significant contact angle change can be as large as several hundreds of volts [15, 16].

Notes that for the goal of this project, a prosthetic eye with dilating pupil, such high voltages are not allowed, both for patient safety and from an energy point of view. Referring to the **Equation 3.1** and **3.2**, there are four basic clues for low-voltage EWOD design. First, a large initial contact angle θ_0 means a maximum contact angle variation. Second, using thin dielectric materials with high dielectric constants is the most popular method to lower the required voltages [17, 18]. Furthermore, scaling the surface tension γ_{sl} between the solid and

liquid through surface active additives like SDS (sodium dodecyl sulfate), therefore decreasing γ_{lv}, also provides a method to reduce the voltage requirements [19, 20].

To obtain large contact angles at zero voltage, highly hydrophobic insulators should be used. However, this kind of material, should preferably also have a high dielectric constant which limits the required electric field to generate the appropriate surface charge and so the probability of electric breakdown. These requirements largely limit the choice of materials. Furthermore, it is difficult to apply these, usually organic, materials in very thin layers with homogenous thickness and without pinholes or other defects. These non-uniformities may lead to dielectric breakdown. Therefore often a two-layer dielectric approach is used where an inorganic dielectric, with superior insulation properties is applied beneath the hydrophobic layer. This inorganic layer will prevent any current flow and so destructive breakdown of the top-layer. This approach not only allows a more separate optimization of dielectric and hydrophobic properties, but also provides higher capacitance so that lower voltage and potentially greater reliability.

So, in this section, several methods to reduce the required voltage will be theoretically analysed:

- Understand the effect of using the hydrophobic layer and choose a proper material;
- Review and select proper dielectric materials with high dielectric constant;
- Explore the effect of surface active additives in reducing the voltage required for electrowetting.

For the goal of this project all the available materials should be transparent when applied as a thin film so that the appearance of the prosthetic eye device can be as natural as a human's.

2.3.1 Hydrophobic Surface

The requirement to obtain maximum contact angle at zero voltage, can be met by hydrophobic insulating polymer. Recent improvements of the hydrophobic insulating materials give chance to decrease the driving voltage dramatically thanks to the advancing processing methods and more alternative materials. These kind of material is mainly organic polymer and candidates used for EWOD include Teflon [21, 22], Parylene C [23], Cytop [19, 24, 25] and FluoroPel [26-28]. These organic compounds can be easily deposited with thicknesses ranging from a few nanometres to micrometres by spin coating or dip coating methods. Apart from being hydrophobic, these materials layers have very small contact angle hysteresis less than 10° for water in air. **Table 2-1** summarizes the properties and specifications of four popular and predominant materials.

Table 2-1 Comparisons of different hydrophobic materials properties

	Teflon AF	**Parylene C**	**Cytop M**	**FluoroPel**
Dielectric constant	1.93	3.1	2.1	2.25
Dielectric strength (kV/mm)	21	260	110	170
Contact angle with water(°)	105	100-110	110-120	110-120
Typical thickness (nm)	20-2000	＞1000	20-100	20-100
Deposition method	Spin-coating	CVD	Spin-coating	Spin-coating

Teflon AF has the lowest dielectric constant (ε_r=1.93) and lowest dielectric strength, which makes it a good material for hydrophobic layer rather than insulating layer cause it cannot provide a large capacitance [21]. But for the thin film thickness below 100nm, it exhibited high porosity and was subject to substantial charge injection which results in poor electrowetting behaviour [23].

Parylene C has the highest dielectric constant of 3.1 as well as the highest dielectric strength among the four materials, so it can also work as a good insulating layer material in EWOD. One important advantage of the Parylene C is that the Chemical Vapour Deposition process allows to form uniform conformal coatings on patterned substrates [9, 26]. However, it is usually deposited with a thickness more than 1μm, therefore a larger voltage need to drive the electrowetting behaviour [23].

Cytop M and FluoroPel 1601 V are promising materials and show very similar properties [21]. Cytop M has been actively employed in recent years [24, 25]. Compared to Cytop, FluoroPel 1601 V has a better dielectric strength and is easier to get in small volume for experiments. Many researchers did experiments with FluoroPel 1601 V and showed potential usage on electrowetting [26-28].

Due to the properties, availability and price, FluoroPel 1601V is finally chosen to use as the hydrophobic material. According to the datasheet given by the company Cytonix® and other researches, FluoroPel 1601V using spin-coating method with 3000 rpm for 30 seconds, and then baking at 120 −160℃ for 20 minutes, to form a later with thickness of 30 to 50 nm and the contact angle of 110°-120° with DI water.

2.3.2 Insulating Dielectric

Compared with hydrophobic layer, the properties of the insulating layers are much more critical. There are two main criteria, derived from **Equation 3.2** directly, to optimization of the properties of the insulating layer in order to realize the low required voltage: first, material with high dielectric constant can provide larger capacitance; second, the insulating layer

should be as thin as possible. Popular inorganic insulator materials introduced mostly by others include silicon oxide [24, 29], aluminium oxide [30-32], silicon nitride [31, 33-35], bismuth zinc niobate (BZN) [36] and bismuth strontium titanate (BST) [17, 37]. The **Table 2-2** summarizes the dielectric properties of these five materials.

Table 2-2 Comparisons of different insulating materials properties

	SiO_2	Al_2O_3	SiN_x	BZN	BST
Dielectric constant	3.8	10	7.8	70-150	200-300
Dielectric strength (kV/mm)	470-670	500-800	500	-	18-54
Deposition method	PECVB LPCVD	ALD	PECVD LPCVD	CSD Sputtering	MOCVD
Deposition temperature (°)	400	200-300	400	700	500

Silicon oxide (SiO_2) as the most frequently used electric insulator in microelectronics and MEMS, offers high electric strength and high chemical stability and reliability. As for the deposition methods, thermal oxidation and PECVD (Plasma Enhanced Chemical Vapour Deposition) are very often used.

Aluminium oxide and silicon nitride both have high dielectric constant and high dielectric strength, showing a balance of strong dielectric strength and lower driving voltage in electrowetting [31]. What is more, ALD (Atomic Layer Deposition) can deposit aluminium oxide at very low temperature environment of approximately 200℃ with a uniform, thin and pin hole free structure [38].

Recently, the family if bismuth zinc niobate (BZN) thin films have appeared as alternative dielectrics as they have a very high permittivity of 70 to 150, depending on composition and crystallization conditions [36]. BZN films have been successfully prepared by CSD (Chemical Solution Deposition) and sputtering methods. However, high temperature annealing (more than 600℃) is required to crystalized the films and achieve the desired dielectric properties [39].

Barium Strontium Titanate (BST) has the significant highest dielectric constant among the given five materials, which promises a lower required voltage than the others [17, 37]. To obtain a thin film with a thickness less than 100nm, MOCVD (Metal-Organic Chemical Vapour Deposition) can be used [40].

2.3.3 Electrowetting Liquid and Surface Active Additives

The electrowetting liquid is most commonly an aqueous salt solution (KCl, NaCl) in de-ionized water (0.01M to 1M) for sufficient conductivity. In some papers [31, 41], it was demonstrated that it is possible to reduce the oil/water interfacial tension from approximately 40mN/m to below 10 mN/m through using Surface active additives. The lower surface tension can reduce the requirement for electrowetting by reducing γ_{lv} according to the electrowetting **Equation 3-2**.

Surface active additives, also known as surface active agent or surfactants, can be used to modify the wetting properties of the liquid and affect the behaviour of droplets in electrowetting system. The most typical example is soap liquid. Surfactants reduce the interfacial tension between liquid and vapour or two liquids by adsorbing at the interface. Investigations and experiments are continuously explored in order to understand the behaviour of water or conductive liquid with surfactants, including anionic surfactant SDS (Sodium Dodecyl Sulfate) [19, 25, 31, 42], cationic surfactant DTAC (Dodecyltrimethylammonium Chloride) [42] and others. **Table 2-3** shows the structures and conductivity of the two surfactants in water compared to KCl solution, and **Figure 2-4** shows the contact angle-voltage results of different droplet of SDS solution, DTAC solution compared with DI water. A significant reduction of operation voltage can be observed.

Table 2-3 Table of surfactants structure and conductivity in water

Surfactant solution	Structure	Conductivity of solution
1 wt% **SDS** in water	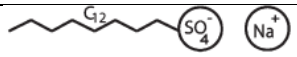	877 µS/cm
1 wt% **DTAC** in water	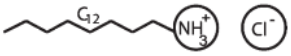	1330 µS/cm
1 wt% **KCl** in water		1002 µS/cm

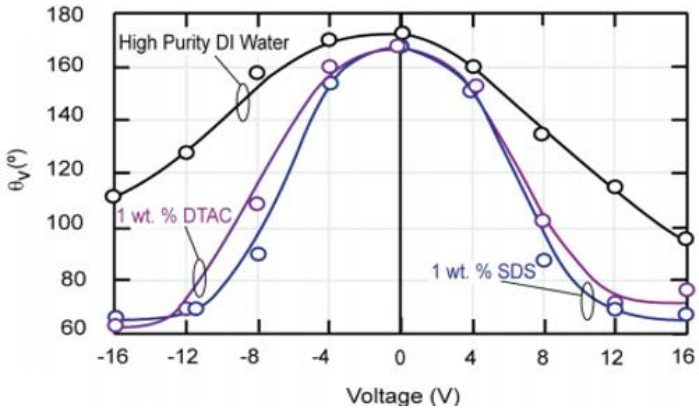

Figure 2-4 Plot of contact angle vs electrowetting voltage for conventional solutions. [42]

When SDS dissolves in water, free ions will be ionized. The small inorganic Na+ ion easily penetrate at the dielectric, whereas the larger dodecyl sulfate ion is clearly less able to penetrate

the dielectric. In [42], it has been consistently seen that electrolysis occurs rapidly for positive bias, but not with negatives bias. While DTAC solutions may have similar problem with negative bias.

2.4 AC vs DC

Electrowetting can be performed well under both direct (DC) voltage as well as alternating (AC) voltages. For a long term application, a DC voltage tends to electrically charge the surface and causes contact angle hysteresis because the pinning effect [43, 44]. In comparison, AC voltage prevents contact angle hysteresis due to altering charging and discharging cycles. And contact angle saturation lowered from 60° to 45° were also observed in [45]. However, from a perspective of power consumption DC operation is more attractive since the charging and discharging cycles in AC operation will dissipate energy.

For AC electrowetting system, the **Equation 3.2** is correct only when the liquid can be treated as a perfect conductor. However, it is reported that at a certain critical frequency f_C the liquid tends to change from conductive to dielectric behaviour [46]. When the frequency is far below f_C liquids behave as perfect conductors; while far above, liquids behave as insulators.

The general AC electrowetting system shown in **Figure 2-5** (a) can be represented in an equivalent circuit as shown in **Figure 2-5** (b). As the liquid droplet is more conductive than the dielectric insulators and the surrounding dielectric ambient, the resistances of the dielectric layer can be considered infinite and only a capacitor left. Then the associated charging time is

$$\tau = R_l(C_l + C_d) \tag{3.3}$$

$$f_C = \frac{1}{2\pi} \cdot \frac{1}{\tau} \tag{3.4}$$

Where τ is the RC charging time constant of the electrowetting system, R_l is the resistance of the droplet, and C_l, C_d are the capacitances of the liquid droplet and dielectric layers respectively. Usually for DI water or other aqueous solutions, f_C is few kHz [43, 47].

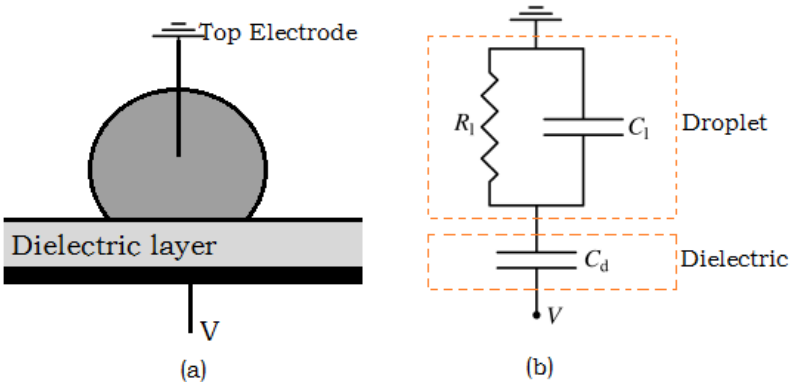

Figure 2-5 (a) A droplet with separate electrodes EWOD configuration (b) equivalent simplified circuit diagram.

The experiments (will be introduced in chapter 5) will comprise both DC and AC operation to see which shows a better overall performance.

2.5 Centralization of the Droplet

Electrowetting experiments are often observed on a horizontal surface rather than a vertical surface. However, the artificial eye is mostly oriented vertical obviously. On a vertical surface, gravity will pull the droplet to move it down. In order to prevent the droplet from sliding down and also fix it in the central part of the prosthetic eye, several methods to eliminate the effect of gravity and to keep the droplet centred are studied.

A method to keep the droplet centred is to bring it in contact with a local hydrophilic surface. Then hydrophilic forces will keep the droplet from drifting aside. Depending on the electrode structure this can be done in two ways: the first is having a hydrophilic top-electrode in contact with the droplet (see **Section 2.5.1**); the other is to open a simple local hydrophilic area in the centre of hydrophobic layer (see **Section 2.5.2**). Although the above measures will keep the droplet centred, some deformation may occur. However, when the droplet is surrounded by an immiscible liquid with approximately the same density, the gravitational force can be largely compensated by the buoyance force [49].

2.5.1 Separate electrodes

The traditional setup for electrowetting has a top electrode inserted to the liquid droplet as the **Figure 2-3** shows. The first method is to make the top electrode insert through the entire droplet as **Figure 2-6** (a).

Applying a transparent lid on the top of whole device to fix the probe electrode standing inside the liquid. Both the probe and the liquid should be black, so from the top, it still looks like the real pupil. And the hydrophilic probe can also provide some stringy force in the interface with liquid droplet, which makes this device gravity-insensitive. The disadvantage of this setup is that the probe electrode may disturb the regular movement of the liquid and have problem of enclosing the top lid perfectly. Another setup can avoid this problem reported in [48] is shown in **Figure 2-6** (b) and (c). In this setup, the probe electrode is made to a patterned electrode on the substrate surface. Making the patterned electrode hydrophilic can make sure the droplet can stay and contacting with on the electrowetting surface. **Figure 2-6** (c) shows the top view of this setup. The top and bottom two connecting parts of the electrode are for connecting of electric voltage. Adding a layer of hydrophobic materials on them can avoid the problem of the liquid deformation.

This two setups gives advantages but still face some difficulties in top electrode fabrication and assembly.

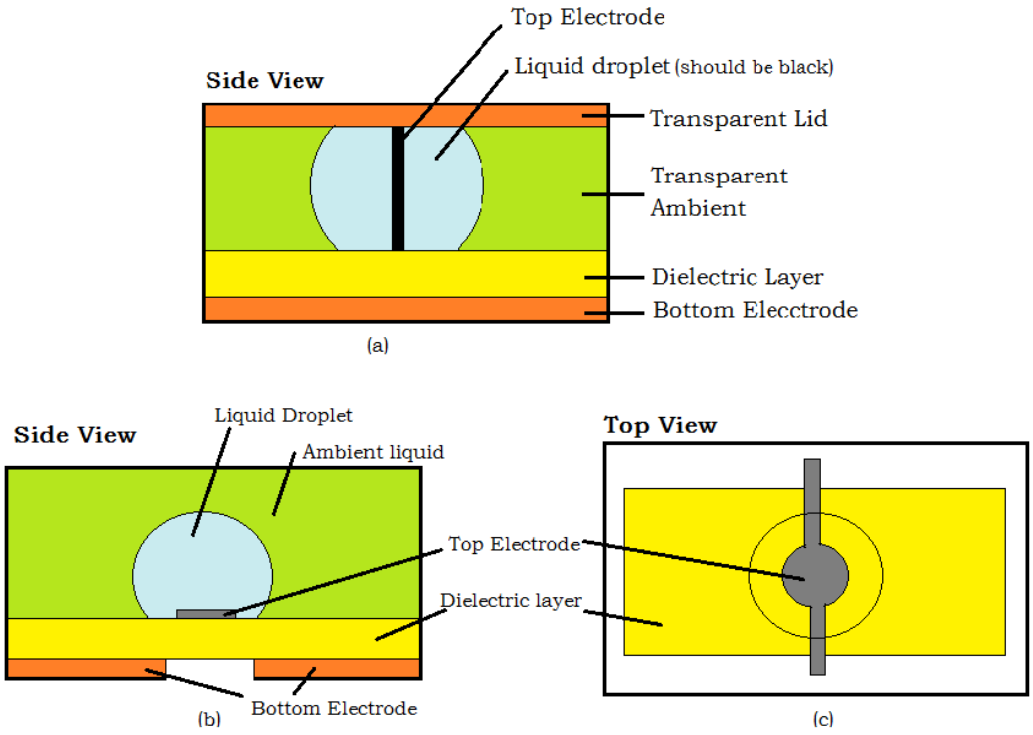

Figure 2-6 (a) side view of the setup with a standing through probe; (b) side view of the setup with a patterned electrode on the substrate; (c) top view of (b), where the outer circle represents the droplet. The two connecting parts should be coated by a hydrophobic layer

2.5.2 Coplanar Electrodes

Except the two separate electrodes setup, an EWOD plate containing both the reference and driving electrodes coplanar has been developed and characterized in [50]. The radial coplanar electrodes is demonstrated in **Figure 2-7** (a). In the presence of an AC applied voltage, the droplet changes its shape and the area covered on the driving and reference electrode (S_A and S_R) changes. Assumed that the droplet is a perfect conductor, the equivalent circuit of the coplanar electrodes can be represented by two variable capacitors C_A and C_R in series as **Figure 2-7** (d) shown. C_A and C_R are the capacitance between droplet and driving electrode and the capacitance between the droplet and reference electrode, respectively. And V_A and V_R are the electric potential of the corresponding electrodes. The two capacitances varies as the contact angle of the droplet changed by the applied voltage. Then the electric potential of the droplet V_L can be calculated from **Equation 3.5**.

$$V_L = \frac{C_A V_A + C_R V_R}{C_A + C_R} \qquad 3.5$$

And the Equation 3.2 can be modified by substituting V with $(V_A - V_L)$, so the relation between contact angle θ and the applied voltage V_A is shown in **Equation 3.6**

$$\cos\theta_{V_A} = cos\theta_0 + \frac{1}{2}\frac{\varepsilon_r\varepsilon_0}{\gamma_{LG}d}(V_A - V_L)^2 \quad 3.6$$

The capacitance is determined by **Equation 3.7.** In this case, since the dielectric constant ε_r is fixed and defined by the dielectric material, the distance d is also fixed by the thickness of the dielectric layer, the capacitance then is only changed by the area *S* of the capacitor. For C_A, it is S_A; and for C_R, it is S_R.

$$\mathrm{C} = \frac{1}{4}\frac{\varepsilon_r\varepsilon_0 \mathrm{S}}{\pi k d} \quad 3.7$$

So if the reference electrode is connected to ground, meaning $V_R = 0V$. The **Equation 3.6** is then represented as:

$$\cos\theta_{V_A} = cos\theta_0 + \frac{1}{2}\frac{\varepsilon_r\varepsilon_0}{\gamma_{LG}d}\left(\frac{S_A}{S-S_g}\right)V_A^{\ 2} \quad 3.8$$

S_g is the gap area between driving electrode and reference electrode. The contact angle changes are related to the area ratio among the two electrodes and the gaps between them. In [51], contact angle changes for EWOD on coplanar electrodes with different gap area 2%, 20%, 40% and 60% were studied and concluded that the highest changes were observed with the smallest gap area 2%.

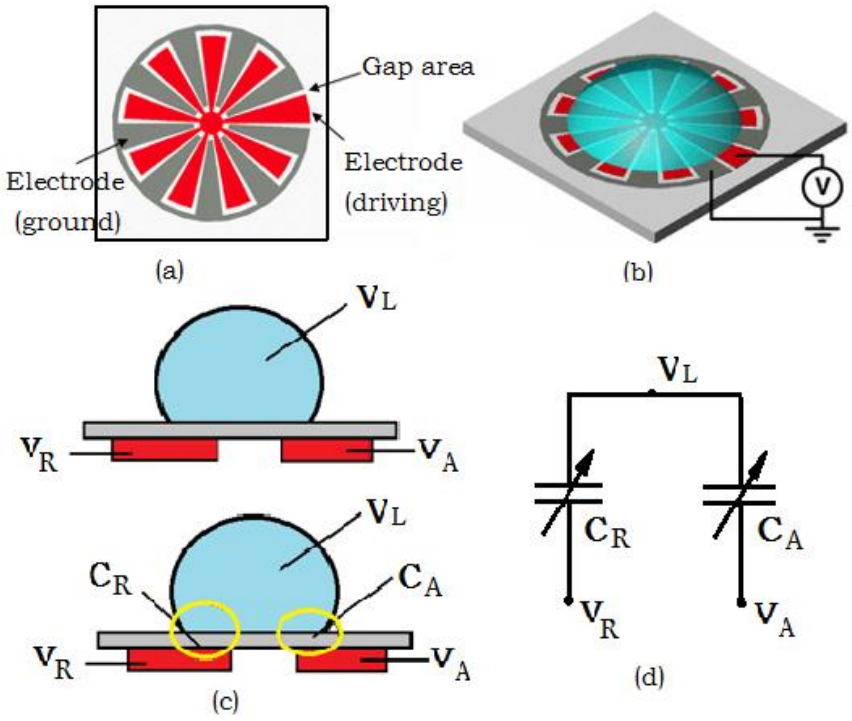

Figure 2-7 EWOD of a droplet on single-side coplanar electrodes: (a) top view of the electrode arrangement [49]; (b) contact angle change with the applied voltage [49]; (c) cross-section view (V_A is the applied voltage, V_R is the ground voltage, V_L is the voltage of the droplet, C_A and C_R is the capacitance of the insulator between droplet and driving electrode or reference electrode, respectively); (d) equivalent circuit.

2.6 Summary

This chapter was mainly divided into two parts. The first part introduced the general background knowledge of electrowetting, including some definitions about wetting phenomenon, brief electrowetting history and theory.

In the second part of this chapter, the approaches to achieve low-voltage electrowetting-on-dielectric device are introduced:

- Using hydrophobic layer material with larger contact angle, using thinner insulating layer with higher dielectric constant and dielectric strength and using liquid with surfactant to lower the surface tension at liquid-vapour interface are the three main methods directly deduced from the electrowetting equation.
- The advantages and disadvantages of AC and DC power supply are analysed.
- From the perspective of application of the device, the ideas of how to fix the droplet in the centre are put forward at last.

Reference:

[1]Wetting. Wikipedia, the Free Encyclopedia. http://en.wikipedia.org/wiki/Wetting (accessed 12 September 2017).

[2]Holder C D. Leaf water repellency of species in Guatemala and Colorado (USA) and its significance to forest hydrology studies. Journal of Hydrology, 2007, 336: 147–154

[3]Holder C D. The relationship between leaf hydrophobicity, water droplet retention, and leaf angle of common species in a semi-arid region of the western United States [J]. Agricultural and Forest Meteorology, 2012, 152: 11-16.

[4]Brewer C A, Nuñez C I. Patterns of leaf wettability along an extreme moisture gradient in western Patagonia, Argentina. International Journal of Plant Sciences, 2007, 227, 168(5): 555–562.

[5]Young T. An essay on the cohesion of fluids [J]. Philosophical Transactions of the Royal Society of London, 1805, 95: 65-87.

[6]Gao L, McCarthy T J. Contact angle hysteresis explained [J]. Langmuir, 2006, 22(14): 6234-6237.

[7]Lippmann, Gabriel. Relations Entre Les Phénomènes Électriques Et Capillaires. Paris: Gauthier-Villars, 1875. Print.

[8]Baird, E., 2007, "Comparison of Electrowetting on Dielectric and Dielectrophoresis Force Distributions," AIAA Paper.

[9]Mugele F, Baret J C. Electrowetting: from basics to applications [J]. Journal of Physics: Condensed Matter, 2005, 17 (28): R705.

[10]Chevalliot S, Kuiper S, Heikenfeld J. Experimental validation of the invariance of electrowetting contact angle saturation [J]. Journal of Adhesion Science and Technology, 2012, 26(12-17): 1909-1930.

[11]Vallet M, Vallade M, Berge B. Limiting phenomena for the spreading of water on polymer films by electrowetting [J]. The European Physical Journal B-Condensed Matter and Complex Systems, 1999, 11(4): 583-591.

[12]Shapiro B, Moon H, Garrell R L, et al. Equilibrium behaviour of sessile drops under surface tension, applied external fields, and material variations [J]. Journal of Applied Physics, 2003, 93(9): 5794-5811.

[13]Makkonen L. A thermodynamic model of contact angle hysteresis [J]. The Journal of Chemical Physics, 2017, 147(6): 064703.

[14]Chang F M, Hong S J, Sheng Y J, et al. High contact angle hysteresis of superhydrophobic surfaces: hydrophobic defects[J]. Applied physics letters, 2009, 95(6): 064102.

[15]high voltage

[16]high voltage

[17]Moon H, Cho S K, Garrell R L, et al. Low voltage electrowetting-on-dielectric[J]. Journal of applied physics, 2002, 92(7): 4080-4087.

[18]Lin Y, Evans R D, Welch E, et al. Low voltage electrowetting-on-dielectric platform using multi-layer insulators [J]. Sensors and Actuators B: Chemical, 2010, 150(1): 465-470.

[19]Berry S, Kedzierski J, Abedian B. Low voltage electrowetting using thin fluoropolymer films [J]. Journal of colloid and interface science, 2006, 303(2): 517-524.

[20]Raccurt O, Berthier J, Clementz P, et al. On the influence of surfactants in electrowetting systems [J]. Journal of Micromechanics and Microengineering, 2007, 17(11): 2217.

[21]Koo B, Kim C J. Evaluation of repeated electrowetting on three different fluoropolymer top coatings [J]. Journal of Micromechanics and Microengineering, 2013, 23(6): 067002.

[22]Zhang H, Weber S G. Teflon AF materials [M]//Fluorous chemistry. Springer Berlin Heidelberg, 2011: 307-337.

[23]Zhou K, Heikenfeld J, Dean K A, et al. A full description of a simple and scalable fabrication process for electrowetting displays[J]. Journal of Micromechanics and Microengineering, 2009, 19(6): 065029.

[24]Berry S, Kedzierski J, Abedian B. Irreversible electrowetting on thin fluoropolymer films[J]. Langmuir, 2007, 23(24): 12429-12435.

[25]You H, Steckl A J. Electrowetting on flexible substrates [J]. Journal of Adhesion Science and Technology, 2012, 26(12-17): 1931-1939.

[26]Dhindsa M, Kuiper S, Heikenfeld J. Reliable and low-voltage electrowetting on thin parylene films [J]. Thin Solid Films, 2011, 519(10): 3346-3351.

[27]Dhindsa M, Heikenfeld J, Kwon S, et al. Virtual electrowetting channels: electronic liquid transport with continuous channel functionality [J]. Lab on a Chip, 2010, 10(7): 832-836.

[28]Banerjee A, Liu Y, Heikenfeld J, et al. Deterministic splitting of fluid volumes in electrowetting microfluidics[J]. Lab on a Chip, 2012, 12(24): 5138-5141.

[29]Heikenfeld J, Dhindsa M. Electrowetting on superhydrophobic surfaces: present status and prospects [J]. Journal of Adhesion Science and Technology, 2008, 22(3-4): 319-334.

[30]Chang J, Choi D Y, Han S, et al. Driving characteristics of the electrowetting-on-dielectric device using atomic-layer-deposited aluminum oxide as the dielectric[J]. Microfluidics and Nanofluidics, 2010, 8(2): 269-273.
[31]Raj B, Smith N R, Christy L, et al. Composite dielectrics and surfactants for low voltage electrowetting devices[C] //University/Government/Industry Micro/Nano Symposium, 2008. UGIM 2008. 17th Biennial. IEEE, 2008: 187-190.
[32]Chang J, Choi D Y, You X, et al. Low voltage electrowetting on atomic-layer-deposited aluminum oxide[C]//Nano /Micro Engineered and Molecular Systems (NEMS), 2010 5th IEEE International Conference on. IEEE, 2010: 612-615.
[33]Acharya B R, Krupenkin T, Ramachandran S, et al. Tunable optical fiber devices based on broadband long-period gratings and pumped microfluidics[J]. Applied physics letters, 2003, 83(24): 4912-4914.
[34]Krupenkin T, Yang S, Mach P. Tunable liquid microlens [J]. Applied physics letters, 2003, 82(3): 316-318.
[35]Cheng J T, Chen C L. Adaptive chip cooling using electrowetting on coplanar control electrodes [J]. Nanoscale and Microscale Thermophysical Engineering, 2010, 14(2): 63-74.
[36]Thayer R L, Randall C A, Trolier-McKinstry S. Medium permittivity bismuth zinc niobate thin film capacitors [J]. Journal of applied physics, 2003, 94(3): 1941-1947.
[37]Liu H, Dharmatilleke S, Maurya D K, et al. Dielectric materials for electrowetting-on-dielectric actuation[J]. Microsystem technologies, 2010, 16(3): 449.
[38]Groner M D, Fabreguette F H, Elam J W, et al. Low-temperature Al2O3 atomic layer deposition [J]. Chemistry of Materials, 2004, 16(4): 639-645.
[39]Ning P F, Li L X, Xia W S, et al. Low temperature crystallized voltage tunable Bi 1.5 Cu x Mg 1− x Nb 1.5 O 7 thin films capable of integration with Au electrode[J]. Ceramics International, 2012, 38(6): 5299-5303.
[40]Okaura S, Suzuki M, Okamoto S, et al. MOCVD growth of Bi1. 5Zn1. 0Nb1. 5O7 (BZN) epitaxial thin films and their electrical properties[J]. Japanese journal of applied physics, 2005, 44(9S): 6957.
[41]Raccurt O, Berthier J, Clementz P, et al. On the influence of surfactants in electrowetting systems[J]. Journal of Micromechanics and Microengineering, 2007, 17(11): 2217.
[42]Raj B, Dhindsa M, Smith N R, et al. Ion and liquid dependent dielectric failure in electrowetting systems[J]. Langmuir, 2009, 25(20): 12387-12392.
[43]Li F, Mugele F. How to make sticky surfaces slippery: Contact angle hysteresis in electrowetting with alternating voltage[J]. Applied Physics Letters, 2008, 92(24): 244108.
[44]Gupta R, Sheth D M, Boone T K, et al. Impact of pinning of the triple contact line on electrowetting performance[J]. Langmuir, 2011, 27(24): 14923-14929.
[45]Chevalliot S, Kuiper S, Heikenfeld J. Experimental validation of the invariance of electrowetting contact angle saturation[J]. Journal of Adhesion Science and Technology, 2012, 26(12-17): 1909-1930.
[46]Chatterjee D, Shepherd H, Garrell R L. Electromechanical model for actuating liquids in a two-plate droplet microfluidic device[J]. Lab on a Chip, 2009, 9(9): 1219-1229.
[47]Hong J S, Ko S H, Kang K H, et al. A numerical investigation on AC electrowetting of a droplet[J]. Microfluidics and Nanofluidics, 2008, 5(2): 263-271.
[48]Zeng H, Feinerman A D, Wan Z, et al. Piston-motion micromirror based on electrowetting of liquid metals[J]. Journal of Microelectromechanical Systems, 2005, 14(2): 285-294.
[49] Bralower H L. A study of electrowetting-assisted boiling[D]. Massachusetts Institute of Technology, 2011.
[50]Yi U C, Kim C J. EWOD actuation with electrode-free cover plate [C]//Solid-State Sensors, Actuators and Microsystems, 2005. Digest of Technical Papers. TRANSDUCERS'05. The 13th International Conference on. IEEE, 2005, 1: 89-92.
[51]Yi U C, Kim C J. Characterization of electrowetting actuation on addressable single-side coplanar electrodes [J]. Journal of Micromechanics and Microengineering, 2006, 16(10): 2053.

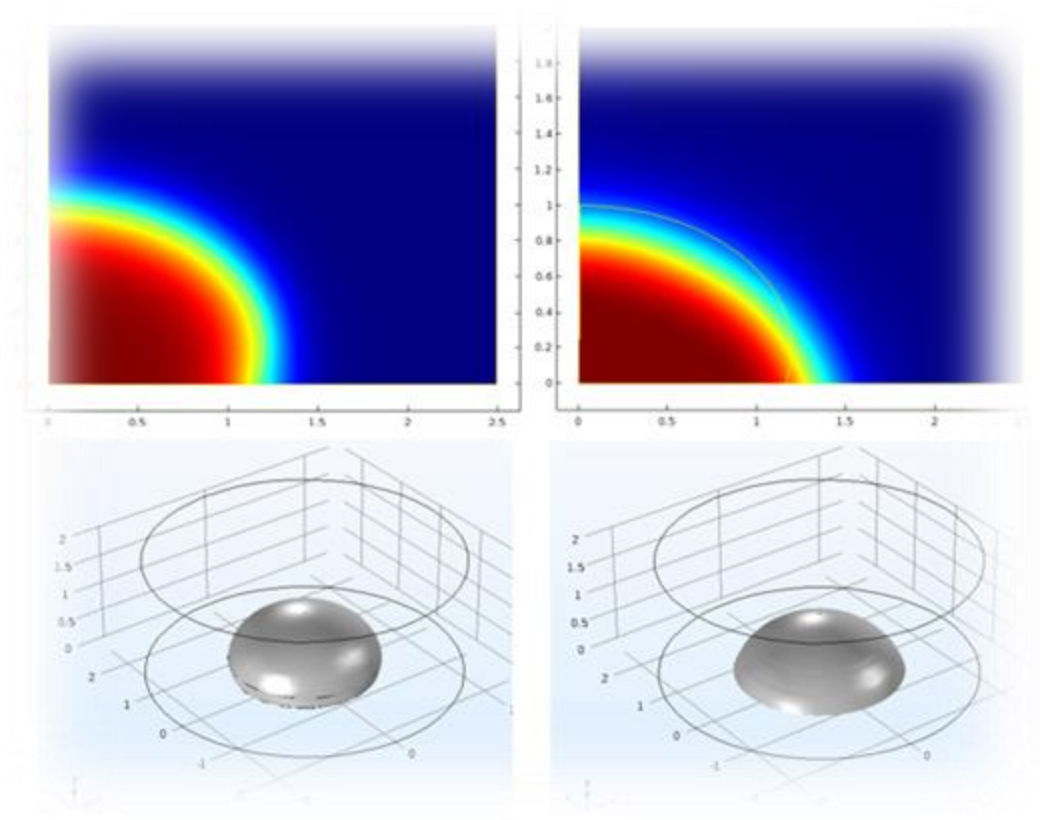

Chapter 3

Modeling of EWOD

In this chapter, Computational Fluid Dynamics (CFD) simulations are demonstrated to study the electrowetting phenomenon of a droplet spreading and contracting on a solid substrate. Two simulation methods are introduced in COMSOL® Multiphysics package for a 2D geometry.

3.1 Introduction of the Model

In COMSOL, two methods are used to get the drop-based electrowetting multi-physics simulation: using the laminar two-phase flow coupled with the level-set physics, the other using a coupled Laminar Two-Phase-Flow (TPF), Electrical Circuit (CIR) and Electrostatic (ES) modules.

1) The Laminar Two-Phase Flow module processes the motions of the interface between two immiscible phases within the framework of Navier-Stokes equations by using the Level-Set method [1].
2) In the second simulation method, the CIR module provides a terminal voltage to the ES module. The ES module solves the Maxwell equations from the voltage input from CIR. The outputs of ES, voltage field, electric field, and electrostatic force, will feed the TPF module. The TPF module solves Navier-Stokes equations and calculates the phase field according to the fluidic boundary conditions [2].

The two methods both solve the Navier-Stokers equations to solve the fluid motion in the model.

A 2D model of a hemispherical droplet is initially placed on a hydrophobic substrate surrounded by air or oil to investigate the motion of the droplet. The droplet is conductive. The simulated geometry is shown in **Figure 3-1**. And the parameters of material physical properties used in the simulation are shown in **Table 3-1**.

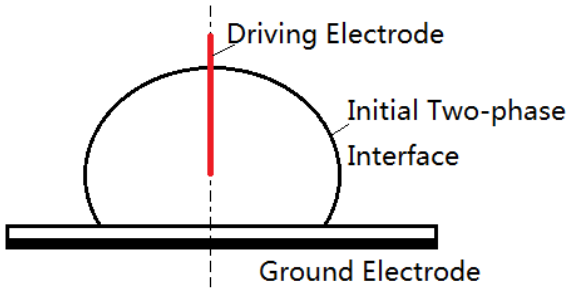

Figure 3-1 A schematic representation of the configuration simulated

Table 3-1 Physical properties of materials typically involved in COMSOL simulations

Material	Density (kg/m^3)	Dynamic viscosity (Pa*s)	Relative permittivity
Water	1000	1e-3	80
Oil	750	0.920e-3	2
Air	0.001	1e-6	1

3.2 Method Ⅰ: Laminar Two-Phase Flow, Level-set Physics

At the beginning, the droplet stays statically on the surface. Under the action of gravity, the droplet is initialized with the contact angle of 130° as the red part shown in **Figure 3-2**. The blue part is defined as oil and the black solid curve represents the initial interface of the water droplet and the oil without the gravity effect.

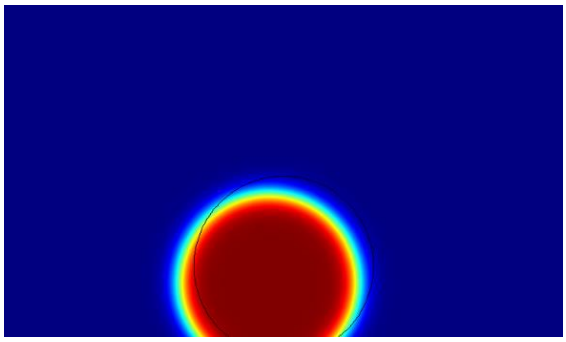

Figure 3-2 Initial contact angle of the droplet (only effected by gravity)

The droplet has a radius of 0.8mm at first. And the surface tension between the water and the oil is 0.05 N/m. The thickness of the dielectric layer is 100nm with a relative dielectric constant of 10. The surface below the droplet is set as the wetted wall. The applied voltage sweeps from 0V to 12V with the step of 1V. When the potential is applied to the electrode under the droplet, a voltage drop across the dielectric layer will lead to changes of the contact angle. The reduction of contact angle makes the droplet oscillate and equilibrate at the final state. By plotting tpf.Vf1 as surface plot, the various stages of the droplet movement at t=0.1s under different applied voltages are shown in **Figure 3-3**.

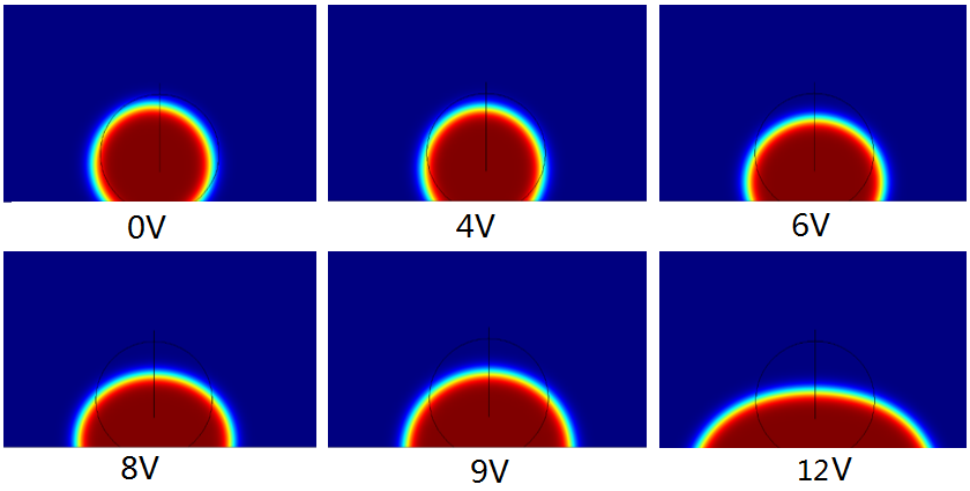

Figure 3-3 Various stages of the droplet shape simulated by TPF physics

The droplet has an apparent movement when 4V is applied. A voltage of 12V creates the smallest contact angle of 50°. The contact angle changes is plotted as a function of the voltage

in **Figure 3-4**. The simulation shows the electrowetting behaviors of the droplet under an ideal and theoretical situation, which will be used to compare with the subsequent experiment results to see the differences.

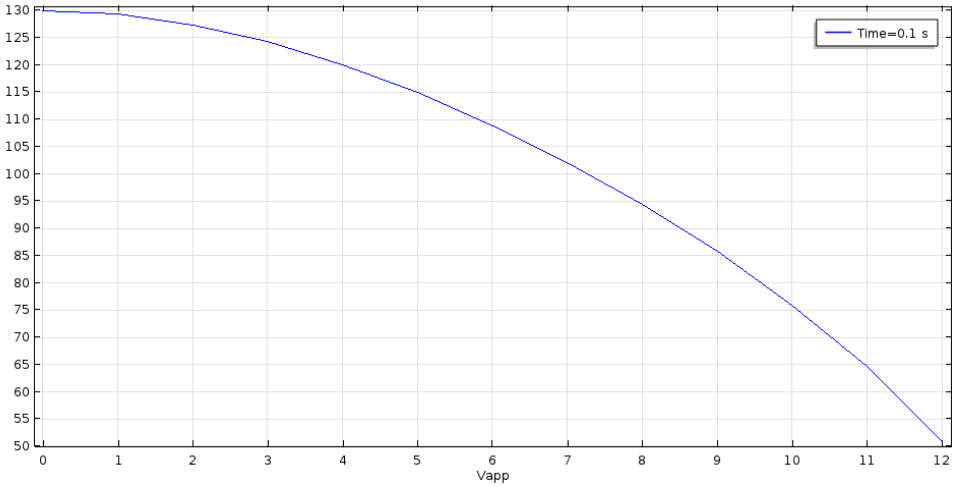

Figure 3-4 Contact angle calculated by the TPF physics as a function of the applied voltage

3.3 Method II: Coupled CIR, ES and TPF Multiphysics

The geometry used for the simulation is a 2D axisymmetric geometry. Revolved around the axis of symmetry, the 3D representation of the results can be easily obtained. The plotted droplet shape compared at time t=0s and t=0.6s is shown in **Figure 3-5**. The dielectric layer is 1μm and relative permittivity of 1.9.

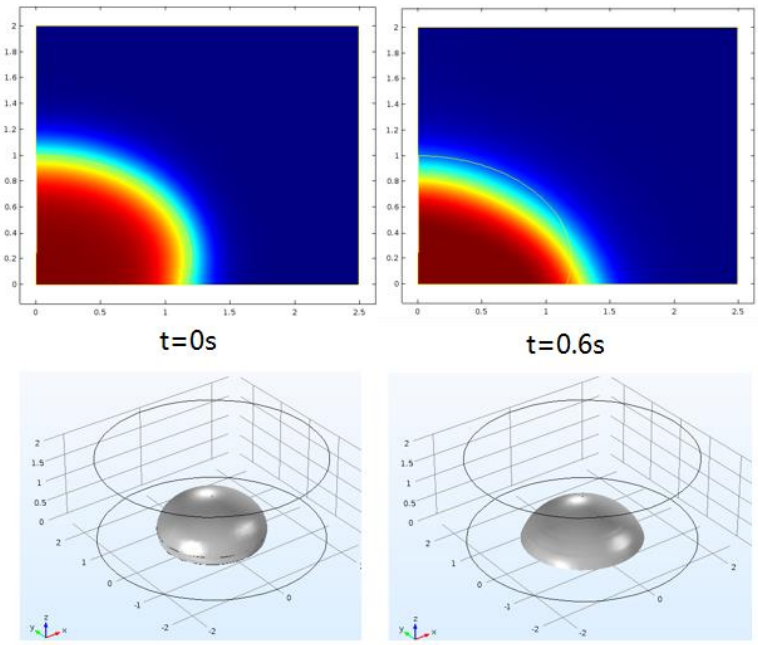

Figure 3-5 The 2D and 3D plots of the droplet shape at t=0s and t=0.6s simulated by CIR, ES and TPF physics for a voltage of 70V

3.4 Summary

In this chapter it was shown how an electrowetting device can be simulated by using the COMSOL® Multiphysics software by two ways: a single physics based electrowetting and a coupled multi-physics simulation. Appendix A describes more in detail the mathematics of the fluid flow modeling and COMSOL commands. The simulation results show that it is possible to manipulate a droplet with relative low voltage.

Reference:

[1] Cahill B P, Giannitsis A T, Gastrock G, et al. A dynamic electrowetting simulation using the level-set method [J]. Proc. of the COMSOL coference, 2008.

[2] Virgilio V. Contactless electrowetting [J]. 2015.

[3] http://www.wright.edu/~nikolai.priezjev/papers/slip_talk.pdf

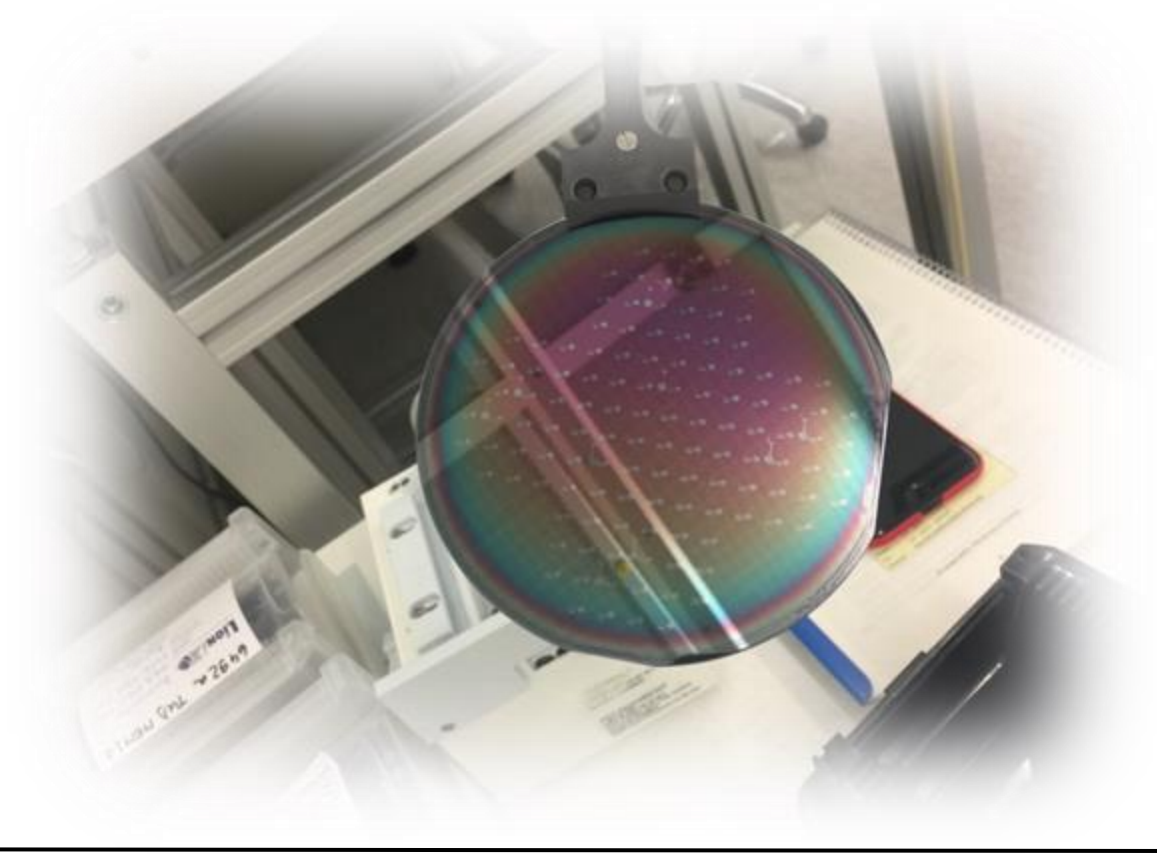

Chapter 4

DESIGN AND FABRICATION

In the previous chapters, low-voltage electrowetting from theory to basic design structure and simulation are discussed. Ways to reduce the required voltage and to center the liquid droplets are also studied. This chapter explains the specific design and fabrication procedure of the device needed to be used in subsequent experiments. Firstly, materials for the electrode, insulating and hydrophobic layer are chosen. Then based on the previous investigation, a mask is designed for fabrication of the different patterned layers. Some of the techniques of fabrication in this project are briefly introduced. Finally, the procedures in the cleanroom are discussed and the fabrication results are shown.

4.1 Material Decision

In chapter 2, materials were listed along with the properties and deposition methods. All the materials are transparent so that the device itself will be transparent too, and can be assembled in the prosthetic eye without influencing the appearance. ITO (Indium tin oxide) glass is transparent and colorless in thin layers [1], which is a perfect and ideal material for electrode. And for insulating and hydrophobic layer Al2O3 (ALD) and FluoroPel 1601V are the best choice among all the alternatives as we discussed in chapter 2.

While for the test and experiment device which will be fabricated in the cleanroom of EKL of TU Delft, it is impossible to deposit transparent conductive material ITO, therefore silicon wafer and platinum are used instead of glass substrate and ITO glass. Besides, the silicon nitride will be tested with different thicknesses to see which combination is better. The materials decided to use are listed in **Table 4-1**.

Table 4-1 Materials, methods and target thickness of each layer

Layer	Material	Method	Target thickness (nm)
Substrate	Silicon wafer	-	-
Electrode layer	Pt	Evaporation	200nm
Insulating layer	SiN Al2O3	PECVD ALD	80nm,100nm 30nm
Hydrophobic layer	Parylene/ FluoroPel	Parylene Deposition/ Spin-coating	50nm 30nm

Noted that silicon is a semiconductor, a layer of oxide is needed to insulate the electrode and the substrate. The target thickness is 500 nm and the deposition method is LPCVD TEOS [3].

4.2 Mask Design

As discussed in chapter 2, the idea of coplanar electrodes is the first choice for our design since it provides a good option to eliminate the top electrode that could disturb the droplet movement. Beside the patterned electrode, the dielectric and hydrophobic layers also need openings for contact bonding (see **Figure 4-1**). Therefore, three masks are required in total for the design.

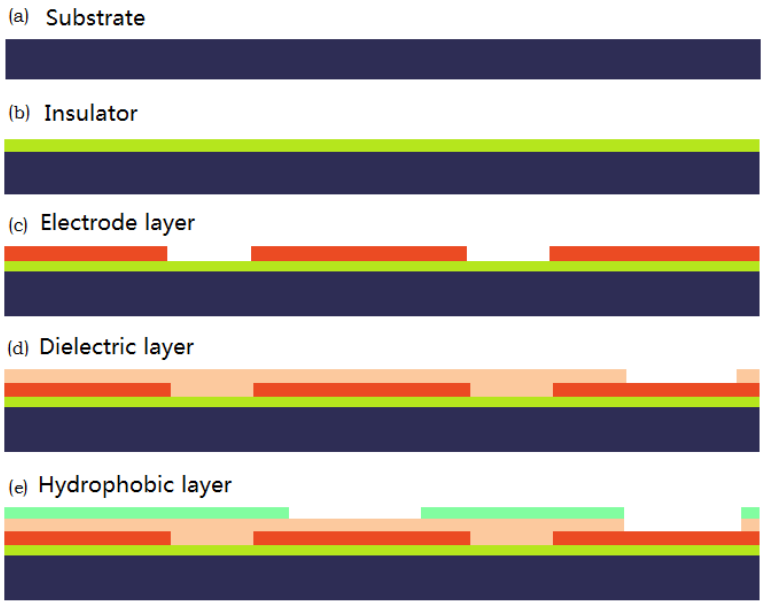

Figure 4-1 The cross section of the multi-layer fabrication steps

4.2.1 Electrode Layer Design

The mask of electrode layer is shown in Figure 4-2. The whole electrodes pattern is designed in radial shape. The red and yellow parts are driving electrode (DE) and reference electrode (RE) respectively. All the reference electrode sectors are connected via an outer ring to a bond pad for external contact. So do the driving electrode sectors. The gap area between reference electrode and driving electrode (5μm) is as small as possible to make it work effectively [2].

Two different sizes of this electrode structure have been designed, one with an outer radius of 1250 μm and the other with 1638 μm radius. Beside the size difference, both electrode designs are identical. **Figure 4-2** shows the smaller version which we call **version one** in the following sections. The bigger one is called **version two**. **Table 4-2** shows the specific figures for the two versions.

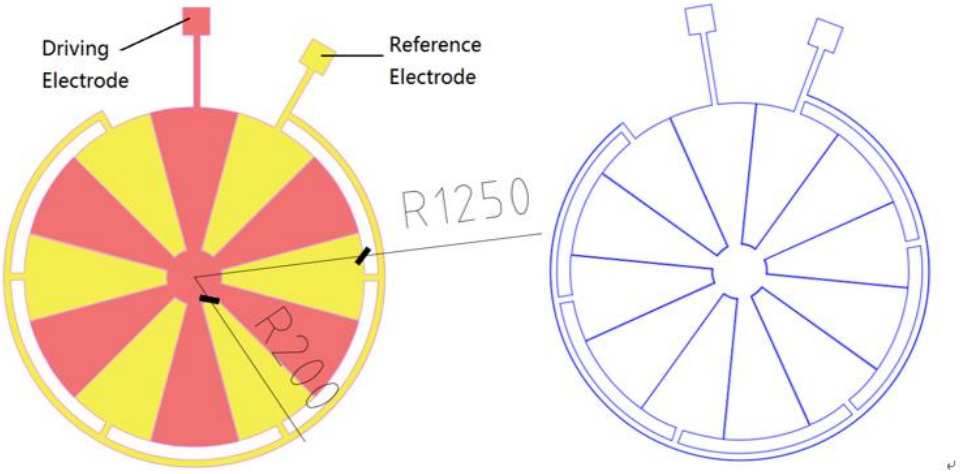

Figure 4-2 Mask for Electrode Pattern Version One

Table 4-2 Numbers of pattern ordered by size (units in µm)

Version No.		Version One	Version Two
Radius 1 (main sectors)		1250	1638
Radius 2 (outer rings)		1400	1834
Radius 3 (center round)		200	262
Gap between DE and RE		5	7
Contact pad edge length		200	262
Via opening edge length		140	215
FluoroPel pattern radius	Overall	1694	1900
	Opening	0	500

4.2.2 Dielectric Layer 'via' Opening

The dielectric layer only needs 2 opening for contact pad. The size is given in **Table 4-2**.

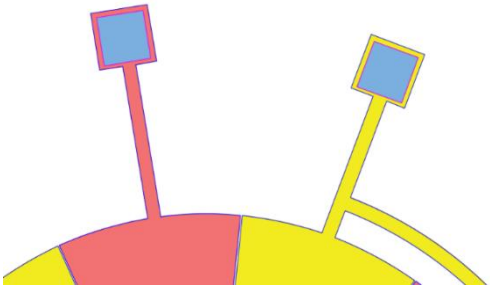

Figure 4-3 Contact 'via' on the mask of dielectric layer (Blue squares).

The microfabrication is designed to deposit a layer of dielectric on the whole surface, then etch the 'via'.

4.2.3 Hydrophobic Layer Design

The mask for the hydrophobic layer are different between the two versions. Version one has a circular area, meaning the surface of the device is hydrophobic everywhere. Version two has an annular area (see **Figure 4-4**), meaning the center has an opening to the dielectric material below which is hydrophilic compared to FluoroPel 1601 V. This hydrophilic area is meant to keep the liquid droplet centered during operation.

Both the masks do not cover the contact pad. The exact dimensions are listed in **Table 4-2**.

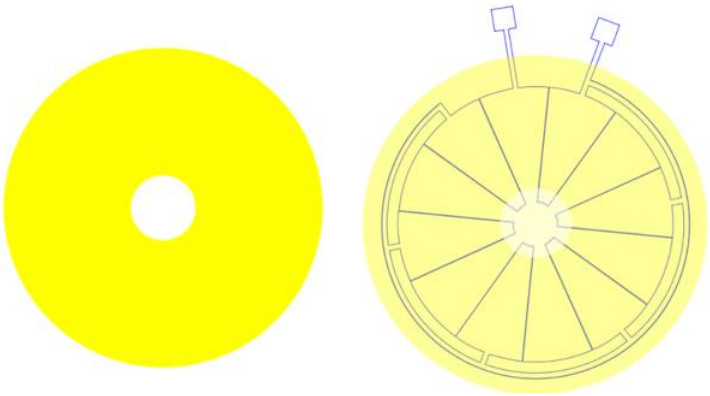

Figure 4-4 Hydrophobic layer mask of version two (Yellow part).

4.2.4 Mask Overview and Creation

The mask was draw in the software *AutoCAD* to create a DXF file, during which it is important to join those lines that belong to the same region into a polyline. Then the DXF file was converted into TDB file by the software package *L-Edit*. The following figures show the design overviews in *L-Edit* for both masks.

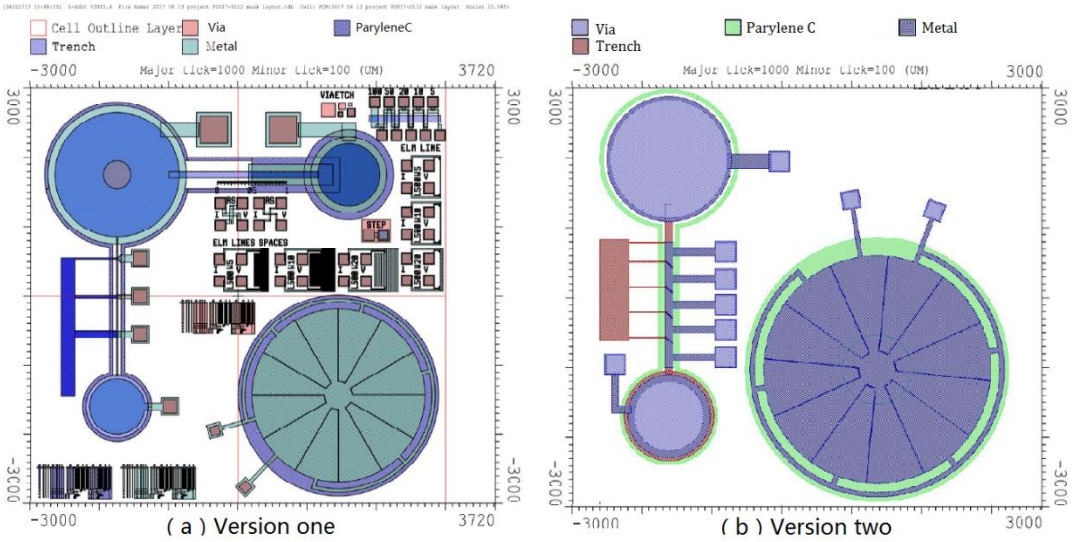

Figure 4-5 The overview of the two designs.

The whole printed mask layout consists of 9 images (see **Figure 4-6**). The patterns on the real mask (see **Figure 4-6** (b)) are 5x larger than on the wafer due to the reduction of the lens of the waferstepper [3, 4]. The images on the mask are 30×30mm, while each device is fitted to a 6×6mm die on a 100mm wafer.

The multi-image mask is shared with another project, the parts marked out by red rectangles are the mask patterns of this project. Image 1-4 are the masks of design version two and image 5-8 are masks of design version one. Some test structures are added with the version one design. In image 9, some auxiliary structures are designed to fill the mask. **Table 4-3** shows the correspondence between design layers and images.

Table 4-3 Each Image Corresponding Layer

Mask Layer	Electrode	Via	FluoroPel	Trench (not this project)
Version One	Image_6	Image_7	Image_8	Image_5
Version Two	Image_2	Image_3	Image_4	Image_1

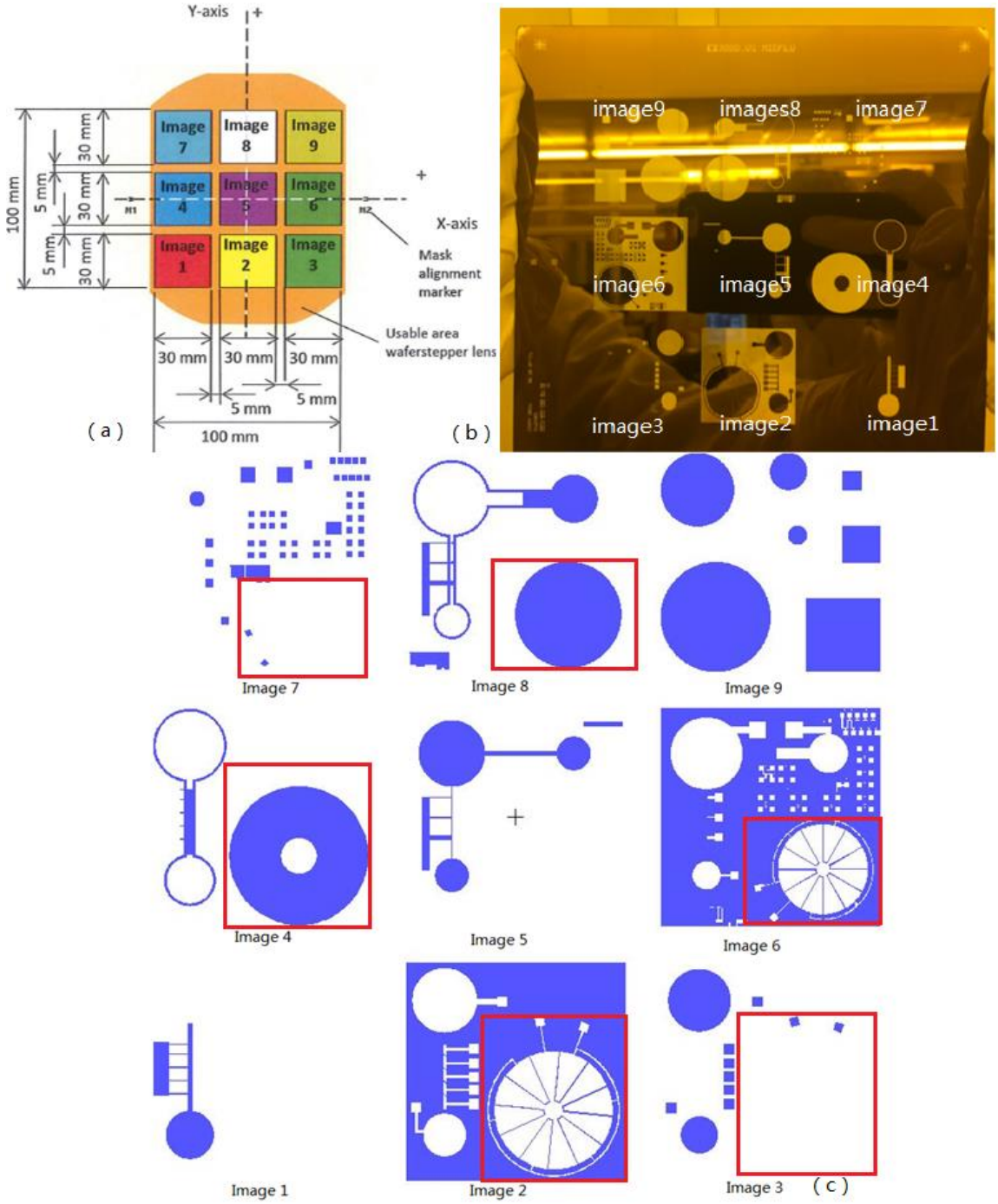

Figure 4-6 (a) Mask layout with dimensions; (b) The mask product used for waferstepper; (c) Mask pattern overview

4.3 Basic Microfabrication Techniques

Before fabrication in the cleanroom. The key concepts and principle and some basic techniques we needed to use in this project are learned: thin films deposition, photolithography, etching as shown in **Figure 4-7**.

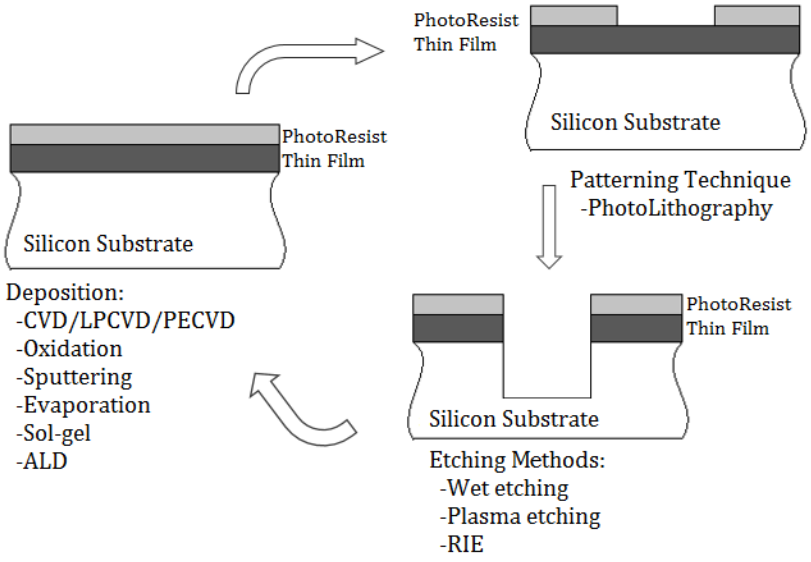

Figure 4-7 Scheme of basic fabrication processes

4.3.1 Photo Lithography

Photolithography is a process used for microfabrication to pattern parts of a thin film or the bulk of a substrate. During this process, a pattern can be transferred from a mask to the surface of the substrate [5]. There are several standard and basic steps in sequence:

- Cleaning: Wafers are cleaned in nitric acid to remove the small and unwanted particle and dirt on the surface.
- Photoresist coating and baking: Photoresist is coated on the surface which will be photo sensitive. This procedure consists of a treatment with HDMS (hexamethyldisilazane) vapor, with nitrogen as a carrier gas, spin coating of photoresist, and a soft baking. HDMS is applied to make the surface stickier to the photoresist. Soft baking is an essential step by which the solvent can be removed and the photoresist becomes photosensitive [6]. (see **Figure 4-8** (1))
- Mask alignment and exposure: Wafers are prepared with alignment makers on the four corners and right and left sides on the front side in the very beginning procedure, which is called zero layer. In this step, a mask is used to precisely align with the makers on the wafer. After aligning, the photoresist is exposed to UV light (see **Figure 4-8** (2)).
- Development: **Figure 4-8** (3) shows the development difference of two very different types of the photoresist: positive or negative photoresist. For **positive** photoresist, the exposed

part will be **removed** by the developer. While for the **negative** photoresist, the exposed part **stays** on the surface.

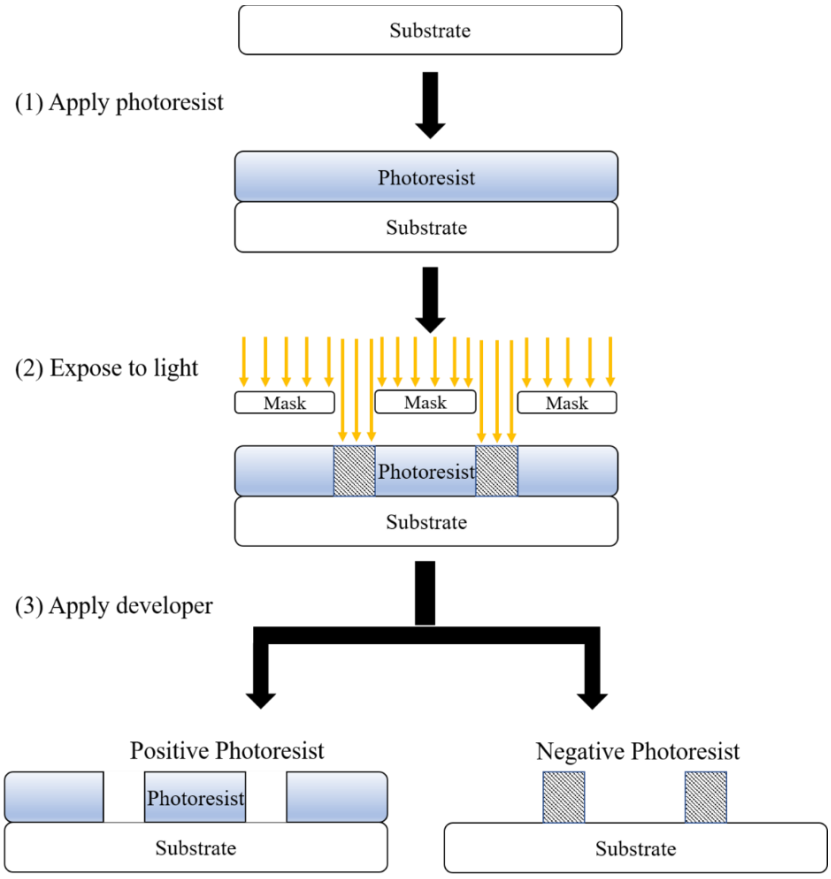

Figure 4-8 Procedures of Photo Lithography [5]

After development, a hard baking step is necessary to harden the photoresist. This step is especially important for negative photoresist [6].

- Photoresist pattern inspection: Inspection of the pattern of photoresist under the optic microscope is to make sure there is no residual photoresist and every structures needed are well standing.

4.3.2 Thin Film Deposition Methods

The thin film is a layer of material ranging from fractions of a nanometer to several micrometers in thickness. The act of applying a thin film to a surface is thin-film deposition. Deposition techniques mainly consists of two broad categories: Chemical Deposition and Physical Deposition, depending on the process is primarily chemical or physical [7]. Here we briefly introduce the methods involved in the next fabrication steps.

LPCVD (Low Pressure Chemical Vapor Deposition) is a chemical deposition technology that uses heat to initiate a reaction of a precursor gas on the solid substrate [8]. This reaction at the surface is what forms the solid phase material. Low pressure is used to decrease any unwanted

gas phase reaction and also increase the uniformity across the substrate surface. Silicon oxide films deposited from TEOS (tetraethyl orthosilicate) is widely used in the semiconductor industry.

PECVD (Plasma Enhance Chemical Vapor Deposition) is also a chemical deposition technology which involved plasma chemical reactions. Plasma is created by means of radio frequency or direct current discharge between two electrodes. The chemical activity of the plasma is high and it is prone to react and deposited on the substrate at low temperature (approximately 400℃) [10]. The silicon nitride dielectric films prepared by PECVD method have many merits, like high reaction rate and good uniformity.

ALD (Atomic Layer Deposition) is also a chemical vapor deposition technology with high potential to produce very thin and conformal films [13]. In ALD, each deposition cycle is divided into four steps: first, a precursor is injected in the deposition chamber. The second step is to remove excess reactant in the chamber with nitrogen or argon. Then the third step is to inject the second precursor into the chamber. In the case of metal oxide layers deposition, this is usually an oxide agent like H2O. And the last step is a second purging gas to remove the excess reactant. In each of this four-step process, the substrate is exposed to two reactants in a sequential and non-overlapping way. The thin film growth can be controlled at 0.1nm per monolayer [14]. Aluminum oxide can be deposited with the ALD system to form a very thin layer with excellent dielectric properties [15, 16].

Thermal Evaporation is a typical physical deposition method. The target material is melted by using an electric resistance heater [17]. In this process, a high vacuum environment is needed to allow vapor to reach the substrate without reacting with gas phase in the chamber.

4.3.3 Etching Methods

Etching is used in microfabrication to chemically remove layers from the surface of a wafer. The two fundamental types of etchants are liquid-phase (‘wet etch’) and plasma-phase (‘dry etch’). Part of the wafer can be protected from the etchant by a masking material like photoresist or silicon dioxide [18]. Organics like photoresist are removed in oxygen plasma or in H2SO4/H2O2 (Piranha) solutions. Oxide or nitride like SiO2 and Si3N4 are etched in CF4/SF6/NF3 plasma [18].

4.4 Fabrication Procedure in the cleanroom of EKL

4.4.1 Introduction

In this section, the details of the fabrication process of the device is discussed. The main process steps to construct the multi-layer device are presented in **Figure 4-9**.

Before every process steps, wafers are cleaned in 100% HNO3 at ambient temperature and 65% HNO3 at 100℃ to remove any dust and small molecules from the surface. The whole fabrication process starts with defining the 'zero layer' marks on bare silicon wafers which will be used for accurate alignment with the masks in the following steps.

The next step is LPCVD deposition of 500nm TEOS oxide, during which the TEOS is deposited on both front-side and back-side. The oxide layer on front side is to insulate silicon and the electrode layer. The oxide layer on the backside can prevent backside contamination with Pt later.

Platinum electrodes are then created via a lift-off process. First a 3.5 μm thickness photoresist is spin-coated on the wafer, patterned via lithography and development. Subsequently a Pt layer is evaporated on top of photoresist pattern. The temperature of the wafer is controlled below 85℃. Finally the lift-off process is applied. An NMP solution is used to dissolve the photoresist, thus removing the unwanted metal on the top of the resist.

Pt can also contaminate the backside of the wafer during the evaporation process, so after coating a new layer of photoresist on the front side, the silicon oxide on the backside is etched using Buffered Oxide Etch (BOE) [19], to remove any contamination on the backside.

In the next step, either PECVD silicon nitride or ALD aluminum oxide is deposited evenly on the whole wafer as the dielectric layer. The wafers are deposited with different insulator thickness（80nm and 100nm silicon nitride and 30nm aluminum oxide). Next the electrode contact openings are plasma-etched.

Finally a layer of FluoroPel 1601V (30nm) is deposited on the top by spin coating. And the openings for electrode contact and the center part are etched by the oxygen plasma.

After all these processed finished, the wafers are diced into small pieces for subsequent packaging wire bonding and experiments.

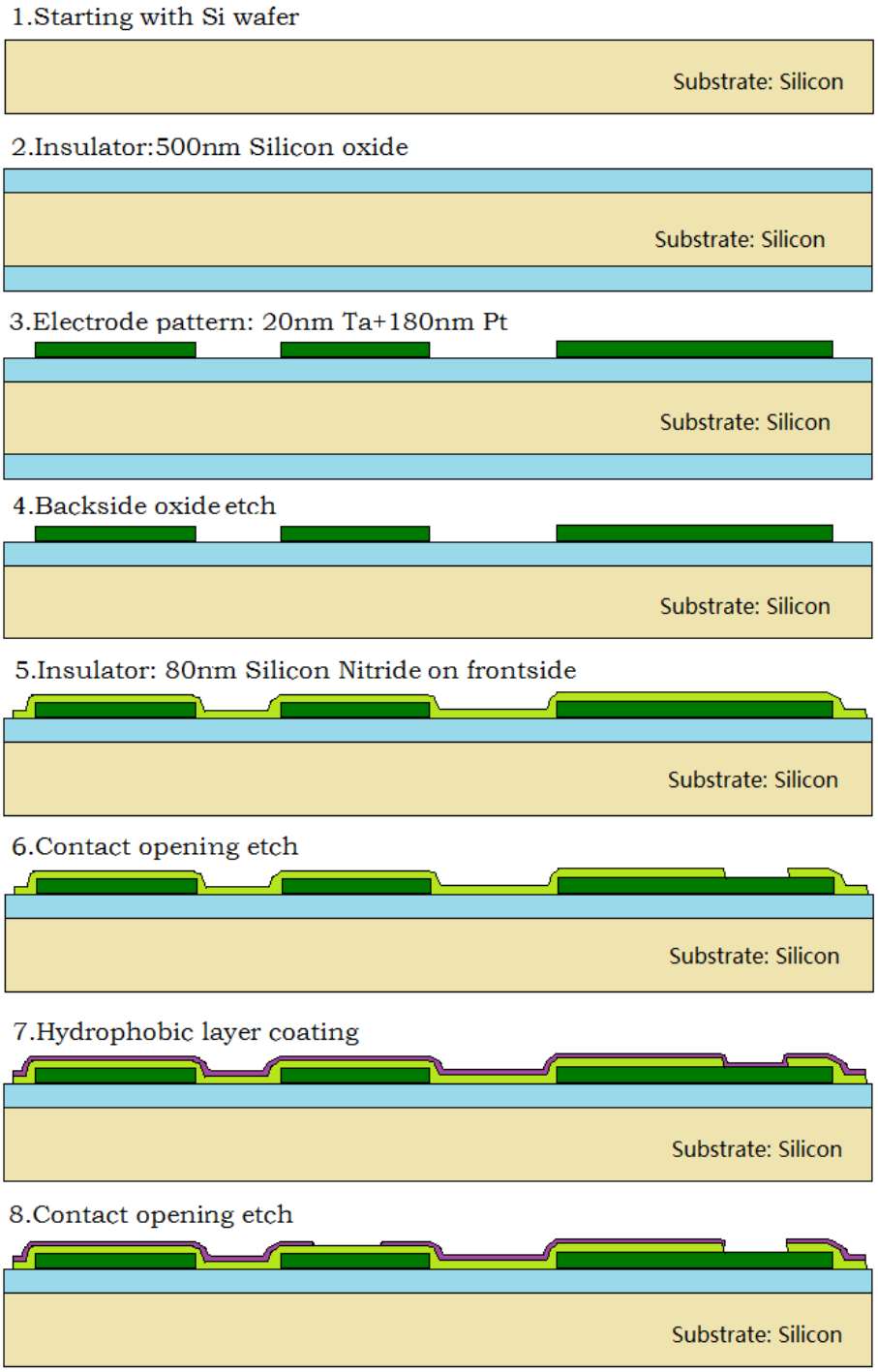

Figure 4-9 The cross-section of main process steps

4.4.2 Cleaning

The objectives of the wafer cleaning process is the removal of chemical and particle impurities without altering or damaging the wafer surface or substrate [20]. The unclean surface can impede the adhesion and uniformity of next deposition materials to the wafer. The steps to clean the silicon surface are the following:

- Cleaning in fuming nitric acid (HNO3 100%) at ambient temperature for 10 minutes;

- Rinse in the Quick Dump Rinser with the standard program until the resistivity is 5 MΩ;
- Cleaning in concentrated nitric acid (HNO3 65%) at 110 °C for 10 minutes;
- Rinse in the Quick Dump Rinser with the standard program until the resistivity is 5 MΩ;
- Drying with the standard program of the Ultra-pure-6 Spin Rinse Dryer.

4.4.3 Zero layer lithography and TEOS deposition

Alignment is a major criterion in all lithography techniques. To align layers accurately, processing usually begins with the zero layer lithography: only alignment marks are exposed on the zero layer and etched directly into the wafer [21]. Then all subsequent masks are aligned to the zero layer marks. This consists of following steps:

- Spin coating the wafers with positive photoresist, and soft baking at 95℃ for 90 seconds;
- Alignment and exposure on the waferstepper;
- Development consists of a post- baking at 115℃ for 90 seconds, developing with MF322 solution, and a hard baking at 100℃ for 90 seconds;
- Writing clear number on the wafers using a quartz pen;
- Plasma etching at 20℃ for 50 seconds to etch 120nm deep structures into silicon;
- Removing the photoresist in an oxygen plasma.

Afterwards, a layer of 500nm TEOS is deposited on top of the silicon using the LPCVD furnace. The layers thickness depends on the deposition time. According to calculation from the average deposition rate during recent usage, the deposition rate at the temperature of 700℃ and pressure of 250mTorr is approximately 0.13 nm/s. So to obtain a 500nm thickness the TEOS deposition needs 1 hour and 5 minutes. The measured results is 478.98 nm.

4.4.4 Lithography, Metallization and Lift Off process

The 'Metal' mask is a closing mask, which means the part need to have metal is solid and the other part is transparent. And the metal part needs to be free of photoresist, so the negative photoresist AZ® Nlof 2020 is spin-coated on the wafer and baked at 100 ℃ for 90 seconds forming a layer with thickness of 3.5 µm. The thicker photoresist can help to achieve a good quality of the lift-off patterns.

AZ® Nlof 2020 is a polymer with longer chains than positive resist. After alignment and exposure with the energy of 50mJ, the **post exposure baking** (performed after exposure, but before development) is essential for the crosslinking, to complete the bonds formed during the exposure. Negative resist at this region becomes insoluble and will not be distorted when developing (see **Figure 4-10**) [22, 23].

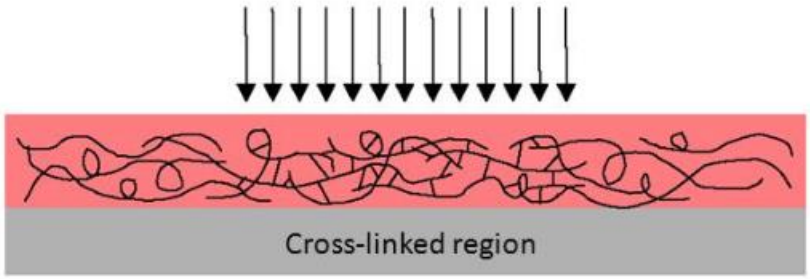

Figure 4-10 Scheme of crosslinking [22]

Once the photoresist is appropriately coated and developed on the surface, the conductive metal Pt is coated onto it with an evaporation machine. Because of the presence of photoresist, the temperature of wafers should not become higher than 85℃. The evaporation process stops manually when the controller reach 80℃, and continues if it is cooled down to 65℃.

The evaporation recipe tried first is **20nm Ta** (tantalum) **and 180nm Pt**. Ta is an additional precursor layer to make Pt stick better to the wafer. Quick visual verification shows good result. The metal seemed shiny and stayed well on the wafers. The other recipe was with **20nm Ti** (titanium) as the additional layer. Also in this case seemed good at first glance. Next, the photoresist and the metal on top of it is removed during the lift off process.

However, the lift off process showed that the adhesion of Ti is bad. The metal peels off from the surface as shown in **Figure 4-11**(c) and (d). Luckily, the first recipe with Ta showed a very good electrode pattern as is shown in **Figure 4-11** (a) and (b).

The backside contamination of Pt can be solved by wet etching the oxide layer using Buffered Oxide Etch (BOE), also known as buffered HF or BHF. The etch rate of oxide is 1.3±0.2nm/s at room temperature. So after about 5 minutes etching, the backside is clean. During this process the front side is protected with photoresist that cannot be etched by BOE.

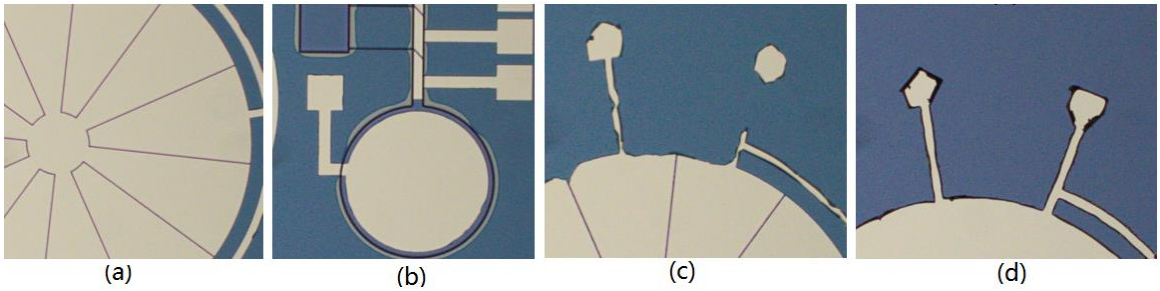

Figure 4-11 Metal lift-off results

4.4.5 Dielectric Deposition and Etching

The Silicon Nitride layer acts as the dielectric between the surface where the droplet rests and the electrode. For the purpose of low operation voltage requirement, and also based on the results of our previous experiments, a layer with thickness of 80nm is thin enough to guarantee low voltage and also thick enough to prevent dielectric breakdown. The PECVD method is fast and low-temperature and can deposit a thin film with only few pinhole. The process temperature is under 400℃.

According to the deposition rate calculated from recent usage, the time to obtain 80nm is about 3 seconds. We also use a bare silicon wafer for measurement the thickness, which showed to be 87nm. To etch the contact opening, the other parts are coated by photoresist first. Then the silicon nitride is etched in **CF4/SF6/O2** plasma for 90 seconds. **Figure 4-12** shows the etching results.

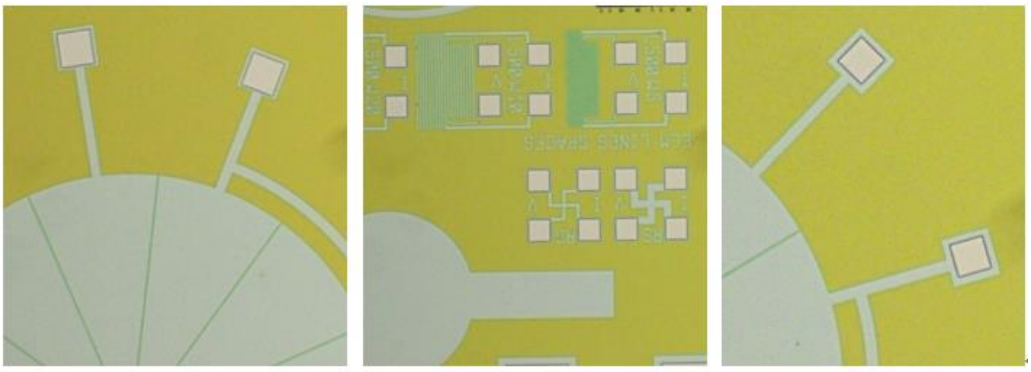

Figure 4-12 Plasma etching results of contact opening on dielectric layer

4.4.6 FluoroPel 1601V Patterned method

The final fabrication step is to coat the hydrophobic material on the top of dielectric layer. The hydrophobic layer is designed to be a ring pattern for the reason of contacting of the electrodes as well as to create an opening in the center of the device.

The target thickness of FluoroPel 1601V is 30nm (see in Appendix B.2). The easiest method is a lift-off process:

- Coating **positive photoresist** with thickness of 3.5μm (much thicker than FluoroPel);
- Alignment, exposure and development;
- Spin coating FluoroPel 1601V on top at 3000 rpm for 1 minute, and baking at 80℃ for 10 minutes and 160℃ for 10 minutes;
- Lift off the resist in acetone.

The adhesion of FluoroPel on silicon nitride is not good enough to withstand the lift-off process. The acetone tears the film off from the surface, as can be seen in **Figure 4-13**.

Figure 4-13 Dipping in the acetone, the whole layer of FluoroPel peels off

So the lift off method is not suitable for FluoroPel patterning. The second method tired is first to coat the wafer a layer of FluoroPel and then etching the FluoroPel with oxygen plasma. This is because FluoroPel 1601V mainly consists of polychlorotrifluoroethylene (PCTFE) which is an organic polymer just like Parylene.

After FluoroPel coating, the contact angle is measured to be 110°. And this hydrophobic surface leads to failures in photoresist spin coating. Therefore, we try to spray coat **negative photoresist** on it. As can be seen in **Figure 4-14**, after 1 layer of spraying, there are lots of bubbles and holes on the surface especially in the center. Totally 3 layers resist are sprayed on it. Nevertheless, still some small pinholes exist.

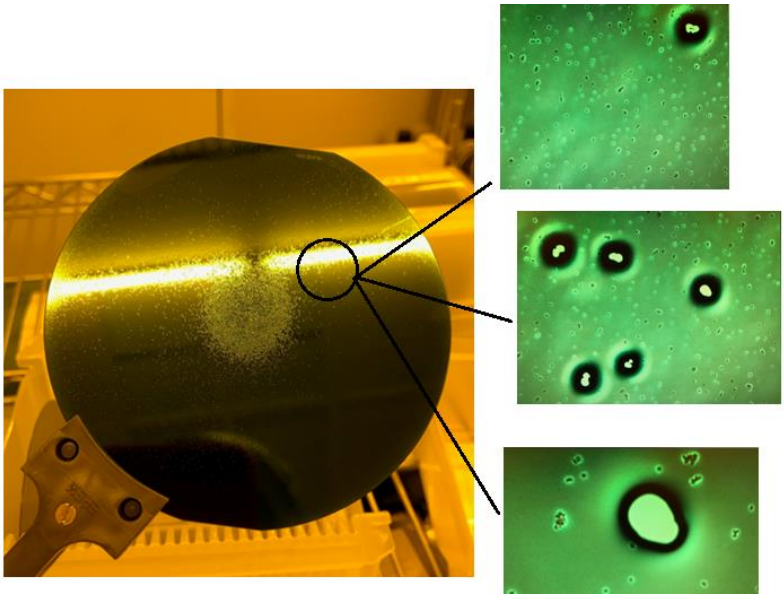

Figure 4-14 Bubbles and holes on spray coated Photoresist results (1 layer)

Another negative photoresist coating method is spin-coating with stickier photoresist Nlof 2070. Making a big puddle on the wafer to cover all the structures and letting it rotating

slowly for a longer time (15s) can make the resist stay on the FluoroPel film, and then it can reach higher speed of 3000rpm for 30s to get a thick resist film about 7-10μm.

Due to the poor adhesion of resist on FluoroPel and the thick layer of resist applied, 7 minutes development makes some small structures at the outside of the wafer disappear. But most structures are still intact. After oxygen plasma etching for 30 seconds, the results seems quite satisfactory. In **Figure 4-15**, the hydrophobic and hydrophilic area are obvious.

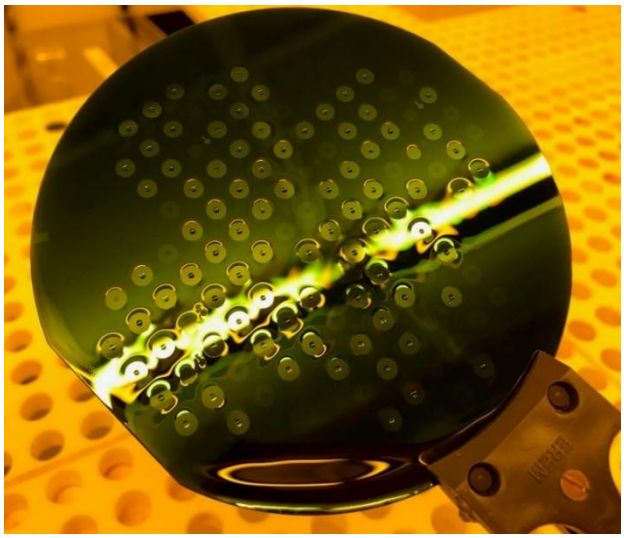

Figure 4-15 after rinsing with water, the hydrophobic and hydrophilic area can be seen

Reference:

[1] https://en.wikipedia.org/wiki/Indium_tin_oxide

[2] http://iopscience.iop.org/article/10.1088/0960-1317/16/10/018/meta

[3] http://www.smfl.rit.edu/pdf/manual/Manual_ASML_Stepper.pdf stepper

[4] https://people.rit.edu/lffeee/Lithography-ASML.pdf stepper

[5] https://en.wikipedia.org/wiki/Photoresist photoresist

[6] https://www.microchemicals.com/technical_information/photoresist_baking.pdf baking

[7] https://en.wikipedia.org/wiki/Thin_film thin film

[8]http://lnf-wiki.eecs.umich.edu/wiki/Low_pressure_chemical_vapor_deposition LPCVD

[9] https://en.wikipedia.org/wiki/Tetraethyl_orthosilicate TEOS

[10] https://en.wikipedia.org/wiki/Plasma-enhanced_chemical_vapor_deposition

[11] Riley F L. Silicon nitride and related materials [J]. Journal of the American Ceramic Society, 2000, 83(2): 245-265.

[12]https://dspace.library.uu.nl/bitstream/handle/1874/668/c4.pdf;jsessionid=974005B9EEEFBE6891A4942985B02A95?sequence=10

[13] https://en.wikipedia.org/wiki/Atomic_layer_deposition

[14] Marin E, Lanzutti A, Guzman L, et al. Corrosion protection of AISI 316 stainless steel by ALD alumina/titania nanometric coatings[J]. Journal of coatings technology and research, 2011, 8(5): 655.

[15] Widjaja Y, Musgrave C B. Quantum chemical study of the mechanism of aluminum oxide atomic layer deposition[J]. Applied Physics Letters, 2002, 80(18): 3304-3306.

[16] Saint-Cast P, Benick J, Kania D, et al. High-efficiency c-Si solar cells passivated with ALD and PECVD aluminum oxide[J]. IEEE Electron Device Letters, 2010, 31(7): 695-697.

[17] https://en.wikipedia.org/wiki/Evaporation_(deposition)

[18] https://en.wikipedia.org/wiki/Etching_(microfabrication)

[19] https://en.wikipedia.org/wiki/Buffered_oxide_etch

[20]http://www.meillc.com/wet-processing-applications/silicon-wafer-cleaning

[21] Franssila S. Introduction to microfabrication [M]. John Wiley & Sons, 2010.

[22] http://slideplayer.com/slide/4502986/

[23]http://newscenter.lbl.gov/2014/07/15/fundamental-chemistry-findings-could-help-extend-moores-law/

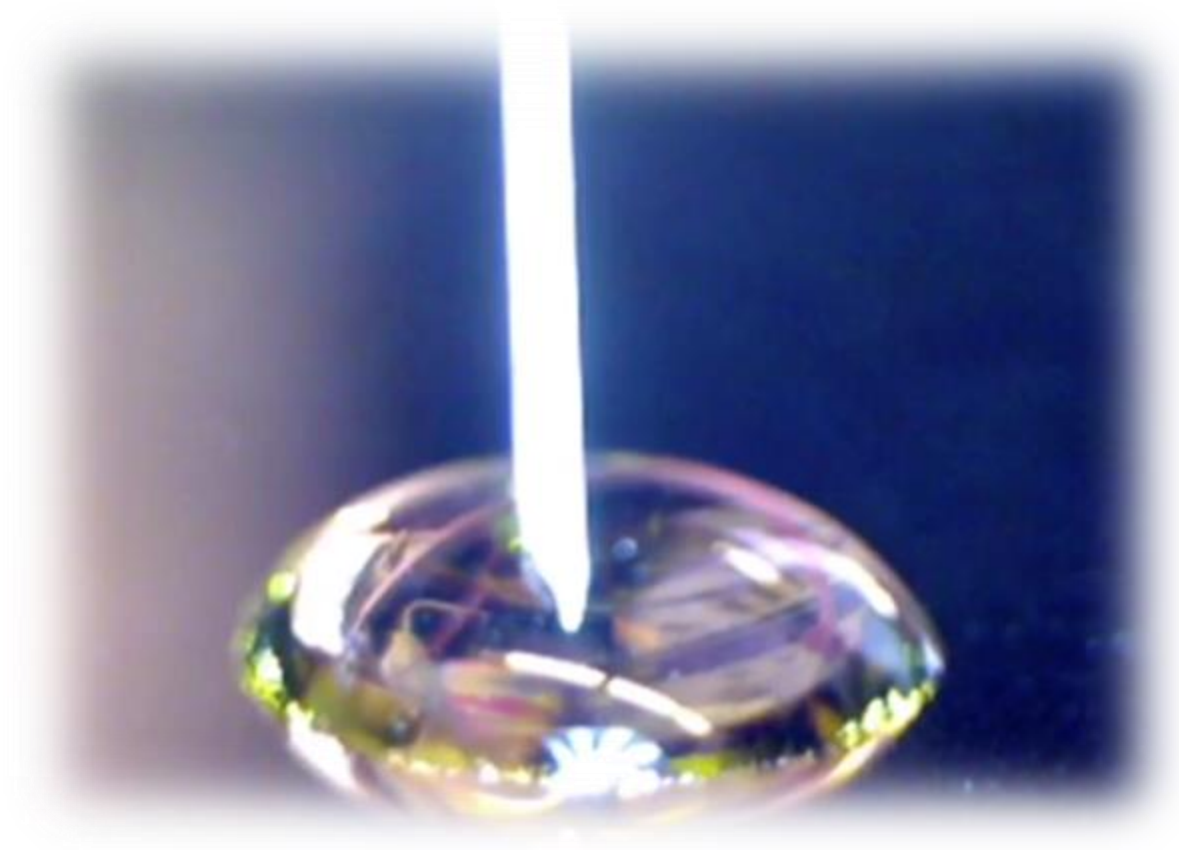

Chapter 5

Experiments and Results

In the previous chapter the design and fabrication processes were described. In this chapter, real-world electrowetting experiments performed on the fabricated devices will be described.

A very simple electrowetting experimental setup was introduced first in order to test the different materials. In this experiment two wafers with different thicknesses of silicon nitride as dielectric layer have been tested to see the influences of the thickness. The second experiment was performed on the final device with coplanar electrodes. Two kinds of dielectric materials as well as different liquid compositions were tested. At last, a long-term experiment to determine the reliability of the FluoroPel thin film was demonstrated.

5.1 Experiment Ⅰ: Testing the electrowetting properties of the selected materials

This first experiment was to test the suitability of the different materials with the setup shown in **Figure 5-1**. The test wafers were obtained from EKL cleanroom. The dielectric material used is PECVD silicon nitride with thicknesses of 102nm and 155nm. On top of it is a layer of spin-coated FluoroPel 1601V (~28nm).

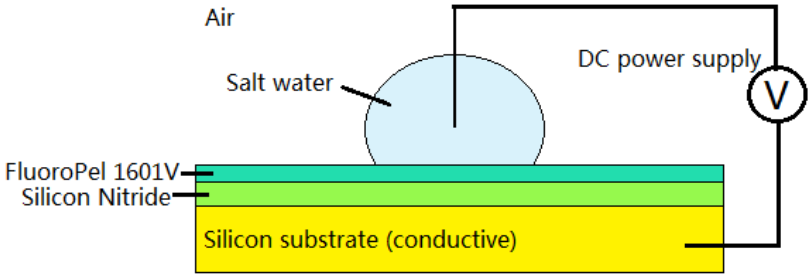

Figure 5-1 Set up of the test of different thicknesses of dielectric

Salted DI water (1% NaCl solution) was used as the electrowetting liquid surrounded by air. The initial contact angle is measured by the Dataphysics® Contact Angle System OCA20. The contact angle of DI water on the FluoroPel surface was 110°.

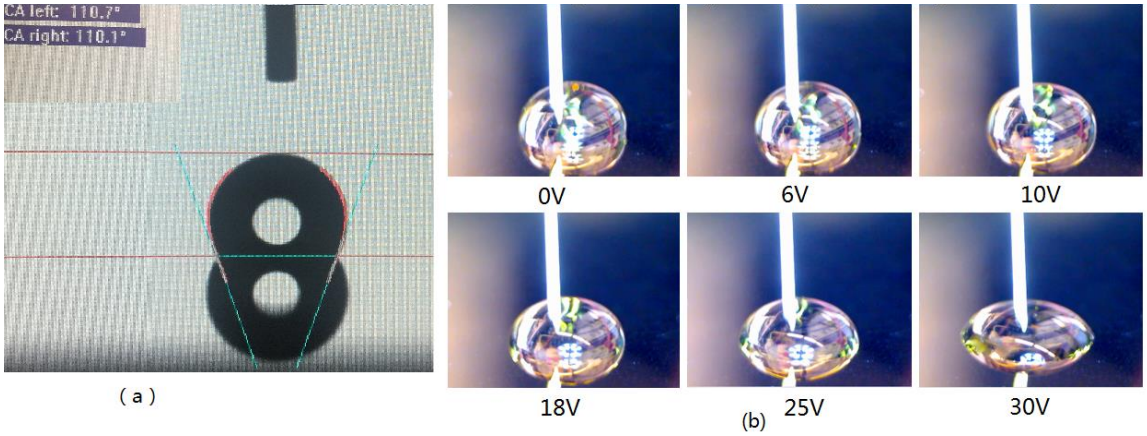

Figure 5-2 (a) Contact angle of DI water on FluoroPel thin film; (b) images of the droplet (NaCl solution) at different voltages (DC)

The results on the two wafers are shown in **Figure 5-2** (b) and **Table 5-1**. For the 155nm silicon nitride one, when the power supply was beyond 6V, the droplet began to move. And from 10V, a bigger contact angle change was observed. Contact angle less than 30° can be seen when the voltage was larger than 28V. Supply voltage exceeding 35V will cause the dielectric to break through. As for the 102nm one, smaller voltages were needed to reach the same state of contact

angle. Interestingly, the small droplet sometimes slipped away to escape from the top electrode when the voltage was larger than 20V.

Table 5-1 Contact angle changes at different voltages of two wafers (DC)

Test Wafer	155nm SiN + 28 nm FluoroPel	102nm SiN + 28nm FluoroPel	Corresponding Contact Angle
Threshold Voltage	6V	4V	110°
Obvious Change	10V	8V	90-100°
The Biggest Change	30V	18-20V	＜50°
Breakdown	35V	-	-

The theoretical breakthrough voltage of the 155nm silicon nitride should be larger than 70V. The test results showed a considerable lower breakdown voltage. The most probable explanation for this is that PECVD silicon nitride is known not to be perfectly free of pin-holes, especially when the layer thickness is less than few micrometer.

5.2 Experiment II: Measurements on the devices with coplanar electrodes

Once the fabrication was finished and the wafer diced in small chips, testing and evaluation were continued. In order to ensure a good electrical contact with the contact pads on the chip, conductive gold wires were used to connect the pads to the DIL24 package (see in **Figure 5-3**)

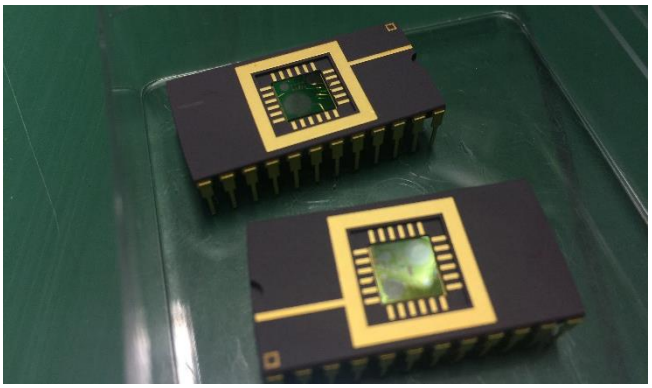

Figure 5-3 Chips in the DIL24 package

The coplanar design allows the two electrodes to be integrate in one plane (metal layer) which makes it more applicable to the artificial eyes. However, the double voltage is needed to drive this device with respect to top-bottom electrode design. Tests on the devices with 87nm silicon nitride showed rather poor performance. Breakdown occurred at rather low voltages from 22V while only a small change in contact angle could be observed. Considering that this voltage is divided over two dielectric layers, the breakdown electric field strength has been reduced to approximately 50% with respect to the first experiment on the 155nm dielectric layer. The

pinholes in the nitride film clearly lead to breakthrough at much lower electric fields when the film thickness decreases.

The experiments of the wafer with 30nm Al2O3 were performed on the probe station without dicing and packaging. The Al2O3 was deposited by the ALD method, so the layer should be free of pin-holes. The expected breakdown voltage of 30nm is 20-24V. The applied voltage was chosen as DC power supply, and the resulting dilation and contraction can be seen in **Figure 5-4**.

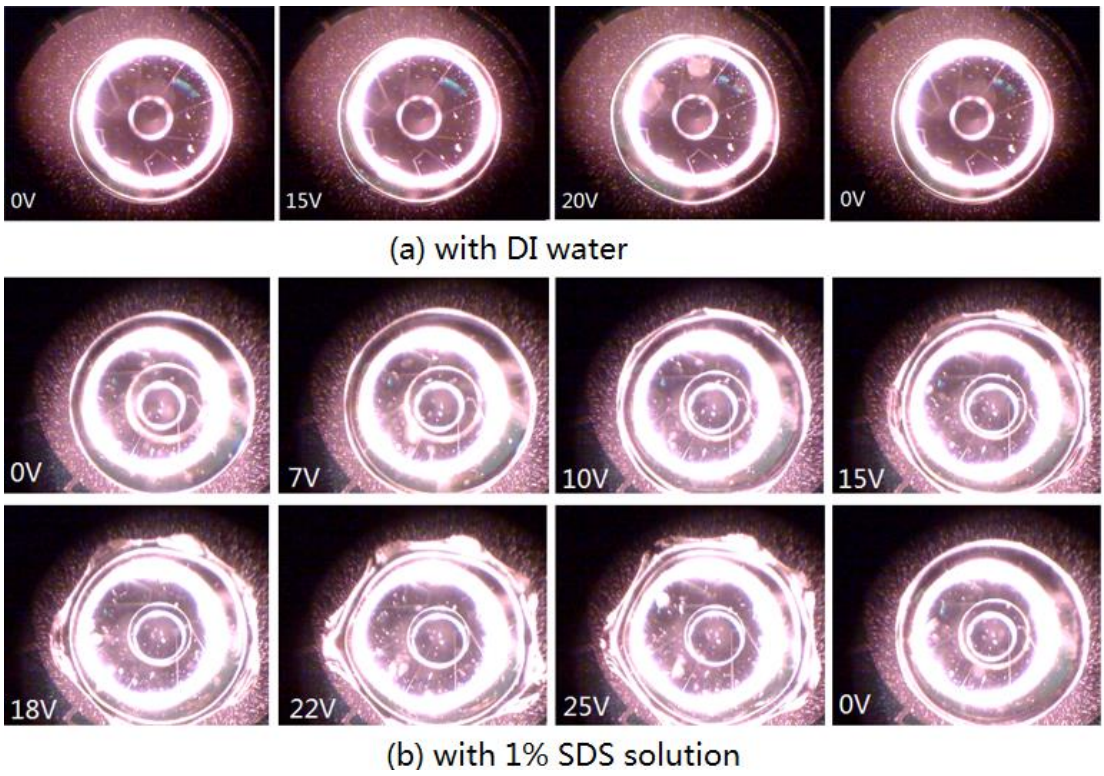

Figure 5-4 Top view of the droplet surrounded by air over 30nm Al2O3 and electrowetting electrodes. (a) DI water droplet images under different voltages (DC); (b) 1% SDS solution droplet images under different voltages (DC).

As expected, the droplet was observed spreading outwards as increasing voltage was applied. **Figure 5-4** shows that the SDS water (1%) required lower voltages than DI water to reach the same contact angle. At the same voltage, the contact angle of SDS water (1%) reduced more.

The Al2O3 dielectric layer broke down for voltages over 25V, which is smaller than the theoretical breakdown voltage, but considering the much thinner layer it performs considerably better than the SiN layer. It should be noted that the FluoroPel layer contributed to the dielectric strength of the device as well. From the **Table 5-2** we can see, PECVD silicon nitride has much lower dielectric strength than the theoretical value, especially when the film thickness decreases due to the increasing influence of pin-holes. Also the Al2O3 layer showed a lower breakdown strength than the theoretical value but performed much better than SiN.

Table 5-2 Comparisons of breakdown voltage of the two dielectric materials and thickness

Material	Thickness	Theoretical breakdown voltage	Experimental breakdown voltage
SiN	155nm	77V	35V
	87nm	44V	11.5V
Al2O3	30nm	20-24V	12.5V

Concerning the planar interdigitated electrode design. Only small variations in droplet size were observed when the voltage was changed. The size variation was considerably smaller compared to the top-bottom electrode test in Experiment I for comparable field strengths. So the electrode design seems not optimal.

5.3 Experiment III: Long-term Test of FluoroPel Reliability

The last experiment was performed on the same wafer as the Experiment I (**Section 5.1**) to test the reliability of the FluoroPel. After six months, the FluoroPel was still as hydrophobic to the water as before. The experiment setup is shown in **Figure 5-5**. In order to make good contact with the wafer, sand paper was used to create an opening for contacting the silicon substrate to the power supply. One electrode was connected to the silicon wafer, the other was inserted into the water droplet. The droplet was surrounded by silicone oil. Then the droplet dilated and contracted as the voltage was changed.

Figure 5-5 Setup pf Long-term experiment on FluoroPel

This experiment lasted for approximately 20 hours. Because the surface was too hydrophobic, the liquid tended to escape from the top electrode. It was not easy to make contact with the droplet. According to the present experimental results, the FluoroPel can maintain its

hydrophobicity for a long time (at least six months) in a passive state while it is reliable in an active cyclic electrowetting test for at least one day.

Chapter 6

Conclusions and Future Works

This chapter concludes the works of this thesis and recommends some improvement ideas for the future work.

6.1 Conclusions

In this thesis, an electrowetting device applied to work as an artificial pupil has been presented from the basic electrowetting theory, simulation, designs, and fabrication processes to the final experiments. The main challenge of this work is to **lower** the voltage requirement of driving the droplet to **dilate and contract** as the human's eye without doing any harm to the users.

Starting from the theory of electrowetting, a series of solutions were discussed. The hydrophobic and dielectric materials chosen to be tested were FluoroPel 1601V, and silicon nitride (PECVD) and aluminum oxide (ALD). And surfactant solution of SDS in water (1%) also provide a solution to reduce the voltage requirement. In order to centralize the liquid, an integrated coplanar electrode and hydrophobic layer with an opening in the center have been designed. Based on the fabrication and experiment results, we can carefully draw conclusions as follows:

- In comparison to PECVD silicon nitride, ALD aluminum oxide showed superior dielectric ability under the tested conditions, even for very thin layers. The results shows that 30nm aluminum oxide can work successfully under the voltage below 12.5V (single dielectric layer) with approximately 40° reduction of the contact angle.
- The experiments on the final co-planar device needed larger voltage than expected from simulation results and simple top-bottom electrode electrowetting experiments, even when corrected for double dielectric layer. It seems that the interdigitated planar electrode design is not an optimal choice with respect to electrowetting sensitivity.
- Surfactants like SDS can lower the surface tension between the droplet and air, which in turn reduce the required voltage. For the same applied voltage of 20V, with SDS solution (1%) the contact angle approximately decreases about 20 degree more than DI water did (see in **Figure 5-4**).
- The long term reliability of FluoroPel was tested in two ways. The FluoroPel layer on the first wafer showed to be stable (exposed to clean air) for more than 6 months. An active operational test (droplet in silicone oil) showed stable electrowetting behavior for approximately 20 hours. As far as the current results are concerned, FluoroPel can provide good long-term stability. Although more research is required to see if it is enough for a dilating pupil.

Although the final device was far from perfect due to several processing issues and the chosen design showed to have a non-optimal electrowetting sensitivity, some solid conclusions can be drawn from the results. The combination of Al2O3 dielectric and Fluoropel hydrophobic layer seems promising to create stable low-voltage electrowetting devices suitable for artificial eyes with dilating pupils. Furthermore a new design based on

one electrode in direct contact with the droplet and the other insulated with the Al2O3/Fluoropel sandwich would be a better configuration.

6.2 Future Work Recommendations

Based on the results of this thesis, some recommendations can be given.

1. Dielectric material

Although ALD deposited Al2O3 seems to be a good candidate since it yields a principally pin-hole free layer with high break-down voltage, other materials with a higher dielectric constant (like BST) could help to further reduce the operating voltage.

2. Electrode design

Concentric electrodes, of which one in contact with the water droplet would have the advantage of higher electrowetting sensitivity at the expense of a slightly more complex production process, i.e. a second metal layer. **Figure 6-1** shows a possible cross-section of such a device (not on scale).

3. Long-term test

Unfortunately the SiN/FluoroPel sandwich was only tested for 20 hours under active electrowetting conditions. In order to draw solid conclusions much longer duration tests are required to see if these materials are able to withstand the very high electric fields and chemicals for a long enough time to allow integration into a prosthetic eye.

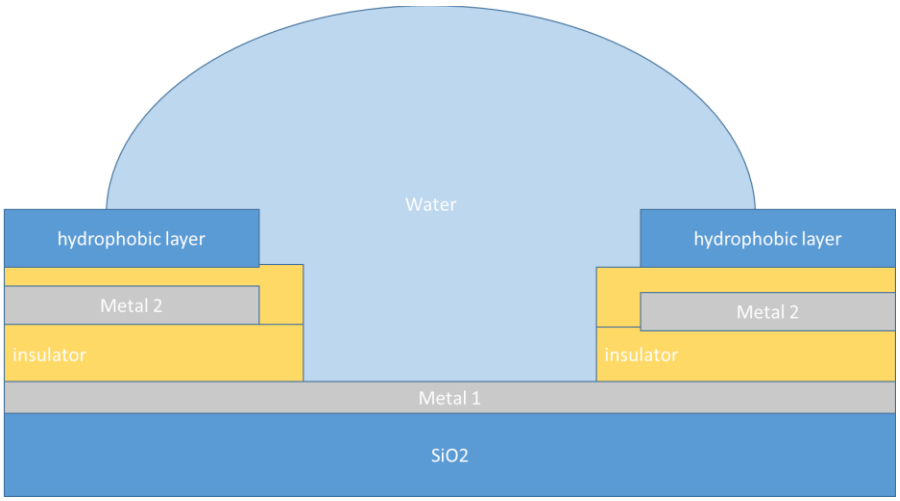

Figure 6-1 Proposed design with concentric electrodes.

Appendix

Process Flowchart

1. CLEANING PROCEDURE: HNO3 100% and 65% (Si) (optional)

Cleaning	10 minutes in fuming nitric acid (Merck: HNO3 100% selectipur) at ambient temperature.
QDR	Rinse in the Quick Dump Rinser with the standard program until the resistivity is 5 MΩ.
Cleaning	10 minutes in concentrated nitric acid (Merck: HNO3 65% selectipur) at 110 °C.
QDR	Rinse in the Quick Dump Rinser with the standard program until the resistivity is 5 MΩ.
Drying	Use the Ultra-pure-6 Spin Rinse Dryer with the standard program.

2. COATING AND BAKING

Use the coater station of the EVG120 system to coat the wafers with photoresist. The process consists of a treatment with HMDS (hexamethyldisilazane) vapor, with nitrogen as a carrier gas, spin coating of Shipley SPR3012 positive resist, dispensed by a pump, a soft bake at 95 ℃ for 90 seconds, and an automatic edge bead removal with a solvent.

Always check the relative humidity (48 ± 2 %) in the room before coating, and follow the instructions for this equipment. Use program "**Co - 3012 - zero layer**". There will be a larger edge bead removal.

3. ALIGNMENT AND EXPOSURE on the PAS5500/80 waferstepper: ZEROLAYERs

Process will be performed on the PAS5500/80 waferstepper

Use COMURK mask, the exposure job: EPI0.0, and exposure energy 150mJ/cm^2

4. WRITE WAFER ID

The lot will be split in the next process flow. Therefore it is important that the wafers are **clearly** numbered. Use a quartz pen to write the wafer numbers in the photoresist. Number the wafers as follows: EI2221-1, EI2221-2, EI2221-3, and EI2221-4.

5. DEVELOPMENT

Use the developer station of the EVG120 system to develop the wafers. The process consists of a post-exposure bake at 115 °C for 90 seconds, developing with Shipley MF322 with a single puddle process, and a hard bake at 100 °C for 90 seconds. Follow the instructions for this equipment. Use program "Dev - SP".

6. INSPECTION: LINEWIDTH AND OVERLAY

Visually inspect the wafers through a microscope, and check linewidth and overlay.

7. DRY ETCHING: URK_NPD

Use the Trikon Ωmega 201 plasma etcher.
Follow the operating instructions from the manual when using this machine.
Use sequence URK_NPD (with a platen temperature to 20 °C) to etch 120 nm deep structures into the Si .

Process conditions of chamber recipe URK_NPD:						
Step	Gasses & flows	Pressure	Platen RF	ICP RF	Platen temp.	Etch time
1. breakthrough	CF4/O2 = 40/20 sccm	5 mTorr	60 W	500 W	20 °C	0'10"
2. bulk etch	Cl2/HBr = 80/40 sccm	60 mTorr	20 W	500 W	20 °C	0'40"

8. RESIST REMOVAL: Tepla

Use the Tepla plasma system to remove the photo resist in an oxygen plasma. Follow the instructions specified for the Tepla stripper, and use the quartz carrier. Use **program 1**

9. CLEANING: HNO_3 99% and 69.5%

Cleaning	10 minutes in fuming nitric acid (Merck: HNO3 100% selectipur) at ambient temperature.

QDR Rinse in the Quick Dump Rinser with the standard program until the resistivity is 5 MΩ.
Cleaning 10 minutes in concentrated nitric acid (Merck: HNO3 65% selectipur) at 110 °C.
QDR Rinse in the Quick Dump Rinser with the standard program until the resistivity is 5 MΩ.
Drying Use the Ultra-pure-6 Spin Rinse Dryer with the standard program.

10. LPCVD DEPOSITION: 500 nm TEOS

Furnace tube: E1 Program name: NEWTEOS1
Follow the instructions for the LPCVD furnace when using this equipment.

Process conditions from recipe NEWTEOS1:			
Gasses & flows	Pressure	Temperature	Time
TEOS bubbler (40 °C)	250 mTorr	700 °C	**variable command**

Note:▪ The layer thickness depends on the deposition time, which can be calculated from the average deposition rate during recent usage.
- An extra test wafer can be deposited for measurements and etch tests.

11. MEASUREMENT: TEOS oxide thickness

Use the Leitz MPV-SP measurement system for layer thickness measurements.
Follow the operating instructions from the manual when using this equipment

12. COATING

Use the coater station of the EVG120 system to coat the wafers with photoresist. The process consists of:
- a treatment with HMDS (hexamethyldisilazane) vapor, with nitrogen as a carrier gas
- spin coating of AZ NLOF2020 negative resist, dispensed by a pump. The approximate spinspeed is 1060 rpm.
- a Soft Bake (SB) at 100 °C for 90 seconds
- an automatic Edge Bead Removal (EBR) with a solvent

Always check the relative humidity (48 ± 2 %) in the room before coating, and follow the instructions for this equipment.
Use program "1-**Co - Nlof – 3,5µm**".

The backside of the wafers should be free of photoresist.

13. ALIGNMENT AND EXPOSURE on the PAS5500/80 waferstepper: METAL

Tool: PAS5500/80 waferstepper
Location: Class 100 Litho room
Energy: 55
Alignment strategy: "GLOBAL"
Settings: no additional user settings are required.
Notes: The chuck-side of the wafers should be free of photoresist and other polymers.

14. X-LINK BAKE

Use the developer station of the EVG120 system to cross link the exposed AZ Nlof 2000 resist. The process consists of:
- A cross-link bake 115℃ for 90 seconds

Always follow the instructions for this equipment.
Use program "**Only – X-link bake**".

15. DEVELOPING

Use the developer station of the EVG120 system to develop the wafers. The process consists of:
- developing with Shipley MF322 with a single puddle process
- a hard bake at 100°C for 90 seconds

Always follow the instructions for this equipment.
Use program "**Dev – lift-off**".

16. INSPECTION: Linewidth and overlay

Visually inspect the wafers through a microscope, and check the line width and overlay. No resist residues are allowed.

17. TEPLA FLASH: Photoresist residues

Strip resist Use the Tepla Plasma 300 system for an oxygen plasma flash.
Follow the instructions specified for the Tepla stripper, and use the quartz carrier.
Use **program 2**: Etch for 1 minute at 600 watts. This will not remove a photoresist masking layer
Note: be sure that the chamber is at room temperature.

18. METALLIZATION: 200 nm Pt

Tool: CHA
Location: CR10000---
Settings: use manual flat alignment to align the flat edge of the wafers
Evaporation of 20 nm Ta and 180 nm Pt 3Å/s in one run with an evaporation starting power of 45%.
Maximum number of wafers 7. Evaporation pressure is < 3.0 E-6 mbar.

The Temperature should not become higher than 85°C.
Remark:
Stop the process on the Inficon IC/5 controller reach 85°C with the stop button.
Continue processing with the the Inficon IC/5 controller start button if the temperature is cooled down to < 65°C.
Use evaporation r**ecipe 11**. Only change thickness value of the Ta and Pt layers

19. INSPECTION: Pattern quality, linewidth and overlay

Visually inspect the wafers.

20. LIFT-OFF MANUAL: NMP

Use the NMP in SAL at 70°C in fume hood to lift-off the metal layer.
Use special glass container with Pt on the sticker.
Heat up the NMP in a beaker filled with water to 70°C in a fume hood.
Put the NMP in an ultrasonic bath. Put the wafers in a holder in the NMP with ultra-sonic on.
Help the lift off process with a Clean tips swabs.
Do not use too much NMP.
Note: There are special bottles for used NMP that could be reused for the lift off process.
NOTE: When finished always turn off the DI-water.

21. INSPECTION: Linewidth and overlay

Visually inspect the wafers through a microscope, No Pt metal residues are allowed.

22. MANUAL COATING: Membranes and Metal Contaminated wafers

Use the Lanz reinraum techniek manual coater system to coat the wafers with XXX.
The process consists of:

- Cover the inside of the coating station with aluminum foil
- Use the membrane chuck for **Contaminated** wafers
- spin coating of XXXX, dispensed by manual or out a syrince

Note: It is not allowed to change parameters of set spin recipes.

23. EXTRA RESIST BAKE

Use the Memmert oven in tunnel 1 to perform an extra resist bake:
⇨ bake the wafers at 140 °C for 30 minutes

24. WET ETCHING: Oxide etch, SAL

USE Special Glass beaker with Pt
Moisten Rinse for 1 minute in wet bench "H_2O/Triton X-100 tbv BHF 1:7". Use the carrier with the blue dot.
The bath contains 1 ml Triton X-100 per 5000 ml deionized water.
Etch Use wet bench "BHF 1:7 (SiO_2-ets)" at ambient temperature,.
The bath contains a buffered HF solution.
Time Etch until the **backside** of the wafer(s) is hydrophobic, plus an extra 30 seconds.
The required etch time depends on the layer thickness and composition.
The etch rate of thermally grown oxide is 1.3 ± 0.2 nm/s at 20 °C.
Rinse Rinse in the Quick Dump Rinser with the standard program until the resistivity is 5 MΩ.
Dry Use the Ultra-pure-6 "rinser/dryer" with the standard program, and the orange carrier with a red dot.

25. REMOVE RESIST WITH FRESH NMP

Use the NMP in SAL at 70°C in fume hood to lift-off the metal layer.
Use special glass container with Pt on the sticker.
Heat up the NMP in a beaker filled with water to 70 C in a fume hood.
Put the NMP in an ultrasonic bath. Put the wafers in a holder in the NMP with ultra-sonic on.
Help the lift off process with a Clean tips swabs.
Do not use too much NMP.
Note: There are special bottles for used NMP that could be reused for the lift off process.
NOTE: When finished always turn off the DI-water.

26. INSPECTION:

Visually inspect the wafers through a microscope, No resist residues are allowed.

27. LAYER STRIPPING: Photoresist

Strip resist Use the Tepla Plasma 300 system to remove the photoresist in an oxygen plasma.
Follow the instructions specified for the Tepla stripper, and use the quartz carrier
Use Special quarts carrier with Pt on it
Use **program 4**: 1000 watts power for 15 minutes.

28. PECVD DEPOSITION: 30 or 80 nm Silicon nitride

use the Novellus Concept One PECVD reactor.
Follow the operating instructions from the manual when using this machine.
It is **not** allowed to change the process conditions and time from the deposition recipe!
Use macro **XXXnmSiNstd** (recipe xxxnmSiNstd) to deposit a chosen thick SiN layer.

Process conditions from recipe 800nmSiN:					
Gasses & flows	Pressure	HF power	LF power	Temperature	Time
$N_2/SiH_4/NH_3$ = 1000/280/1800 sccm	2.8 Torr	320 W	480 W	400 °C	3s

Note: The deposition time is subject to minor changes, in order to obtain the correct film thickness.
Note Use bare silicon wafer for measurement.

29. MEASUREMENT: Silicon Nitride thickness

Use the Leitz MPV-SP measurement system for layer thickness measurements.
Follow the operating instructions from the manual when using this equipment.

30. COATING

Use the coater station of the EVG120 system to coat the wafers with photoresist. The process consists of:

- a treatment with HMDS (hexamethyldisilazane) vapor, with nitrogen as a carrier gas
- spin coating of Shipley SPR3012 positive resist, dispensed by a pump. The approximate spinspeed is 3450 rpm.
- a Soft Bake (SB) at 95 °C for 90 seconds
- an automatic Edge Bead Removal (EBR) with a solvent

Always check the relative humidity (48 ± 2 %) in the room before coating, and follow the instructions for this equipment
Use program "1-**Co - 3012 - 1,4µm**".

31. ALIGNMENT AND EXPOSURE on the PAS5500/80 waferstepper; MASK VIA

Tool: PAS5500/80 waferstepper
Location: Class 100 Litho room
Energy: 300
Alignment strategy: "GLOBAL"
Settings: no additional user settings are required.
Notes: The chuck-side of the wafers should be free of photoresist and other polymers.

32. DEVELOPING

Use the developer station of the EVG120 system to develop the wafers. The process consists of:

- a post-exposure bake at 115 °C for 90 seconds
- developing with Shipley MF322 with a single puddle process
- a hard bake at 100 °C for 90 seconds

Always follow the instructions for this equipment.
Use program "**Dev - SP**".

33. INSPECTION: Linewidth and overlay

Visually inspect the wafers through a microscope, and check the line width and overlay. No resist residues are allowed.

34. PLASMA ETCHING: 50, 100 or 150 nm Silicon nitride

Use the Alcatel GIR300 Fluorine plasma etcher.
Follow the operating instructions from the manual when using this machine.
It is **not** allowed to change the process conditions from the etch recipe, except for the etch time!
Use the process from the table, and **set the etch time to ■'■■**".

Process conditions:					
Step	Gasses & flows	Pressure	RF power	He pressure	Etch time
1. bulk etch (RIE)	$CF_4/SF6/O_2$ = 70/10/10 sccm	0.05 mBar	60 W	not available	**90s**

35. INSPECTION: No residues are allowed.

36. LAYER STRIPPING: Photoresist

Strip resist Use the Tepla Plasma 300 system to remove the photoresist in an oxygen plasma.
Follow the instructions specified for the Tepla stripper, and use the quartz carrier.
Use Special quarts carrier with Pt on it
Use **program 4**: 1000 watts power for 15 minutes.

37. INSPECTION: resist removal

Visually inspect the wafers.
The front and back side of the wafer should be clean of any photoresist residues.

38. Dicing

List of Figures

Figure 1-1 The acrylic artificial eyes with different size, pupil and eye ball colour 2

Figure 1-2 (a) The overview of the LCE (b) Different states of the iris responding to different light power (c) Two boundary states of the pupil: under weak light and strong light. [6] 4

Figure 1-3 An over-sized prototype pupil made from a dielectric elastomer actuator (DEA) [8] 5

Figure 1-4 The show model prototype schematic and assembly (a) The dimension of the iris; (b) Drilled and milled out prosthetic eye; (c) Light sensor placed inside the eye; (d) A hand-painted iris attached; (e) The electrowetting device placed; (f) Side view of the whole prosthetists; (g) The structure and details of the electrowetting device. 6

Figure 2-1 Schematic diagrams of contact angle of a liquid droplet on solid surfaces 10

Figure 2-2 Young's Equation for Three-Phase Interfacial Tension (θ is the contact angle, γsv is the surface tension of solid-vapour surface, γsl is the surface tension of solid-liquid surface, γlv is the surface tension of liquid-vapour surface)..... 11

Figure 2-3 Schematic of electrowetting-on-dielectric. (a, c) No external voltage applied: the droplet is a round shape and contact angle is more than 90 degree. (b, d) External voltage applied: charge density changes so that the contact angle decrease or increase. 12

Figure 2-4 Plot of contact angle vs electrowetting voltage for conventional solutions. [42] 17

Figure 2-5 (a) A droplet with separate electrodes EWOD configuration (b) equivalent simplified circuit diagram. 18

Figure 2-6 (a) side view of the setup with a standing through probe; (b) side view of the setup with a patterned electrode on the substrate;(c) top view of (b), where the outer circle represents the droplet. The two connecting parts should be coated by a hydrophobic layer 20

Figure 2-7 EWOD of a droplet on single-side coplanar electrodes: (a) top view of the electrode arrangement [49]; (b) contact angle change with the applied voltage [49]; (c) cross-section view (VA is the applied voltage, VR is the ground voltage, VL is the voltage of the droplet, CA and CR is the capacitance of the insulator between droplet and driving electrode or reference electrode, respectively); (d) equivalent circuit. 21

Figure 3-1 A schematic representation of the configuration simulated 26

Figure 3-2 Initial contact angle of the droplet (only effected by gravity) 27

Figure 3-3 Various stages of the droplet shape simulated by TPF physics 27

Figure 3-4 Contact angle calculated at the TPF physics in function of the applied voltage 28

Figure 3-5 The 2D and 3D plots of the droplet shape at t=0s and t=0.6s simulated by CIR, ES and TPF physics....28

Figure 4-1 The cross section of the multi-layer fabrication steps....33
Figure 4-2 Mask for Electrode Pattern Version One....33
Figure 4-3 Contact 'via' on the mask of dielectric layer (Blue squares)....34
Figure 4-4 Hydrophobic layer mask of version two (Yellow part). 35
Figure 4-5 The overview of the two designs....35
Figure 4-6 (a) Mask layout with dimensions; (b) The mask product used for waferstepper; (c) Mask pattern overview....36
Figure 4-7 Scheme of basic fabrication processes....37
Figure 4-8 Procedures of Photo Lithography [5]....38
Figure 4-9 The cross-section of main process steps....41
Figure 4-10 Scheme of crosslinking [22]....43
Figure 4-11 Metal lift-off results....43
Figure 4-12 Plasma etching results of contact opening on dielectric layer 44
Figure 4-13 After dipping in the acetone, the whole layer of FluoroPel peels off....45
Figure 4-14 Bubbles and holes on spray coated Photoresist results (1 layer)....45
Figure 4-15 After rinsing with water , the hydrophobic and hydrophilic area can be seen....46

Figure 5-1 Set up of the test of different thicknesses of dielectric 50
Figure 5-2 (a) Contact angle of DI water on FluoroPel thin film; (b) images of the droplet (NaCl solution) at different voltages (DC)....50
Figure 5-3 Chips in the DIL24 package....51
Figure 5-4 Top view of the droplet surrounded by air over 30nm Al2O3 and electrowetting electrodes. (a) DI water droplet images under different voltages (DC); (b) 1% SDS solution droplet images under different voltages (DC). 52
Figure 5-5 Setup pf Long-term experiment on FluoroPel....53

Figure 6-1 Proposed design with concentric electrodes....57

List of Tables

Table 2-1 Comparisons of different hydrophobic materials properties 15
Table 2-2 Comparisons of different insulating materials properties 16
Table 2-3 Table of surfactants structure and conductivity in water 17

Table 3-1 Physical properties of materials typically involved in COMSOL simulations 26

Table 4-1 Materials, methods and target thickness of each layer 32
Table 4-2 Numbers of pattern ordered by size (units in μm) 34
Table 4-3 Each Image Corresponding Layer 36

Table 5-1 Contact angle changes at different voltages of two wafers (DC) 51
Table 5-2 Comparisons of breakdown voltage of the two dielectric materials and thickness 53